Contribution of fine ash to the atmosphere from plumes associated with pyroclastic density currents

Samantha Engwell[1] & Julia Eychenne[2]

[1] Istituto Nazionale di Geofisica e Vulcanologia, Sezione di Pisa, Italy

[2] University of Bristol, School of Earth Sciences, Bristol, United Kingdom

1. Abstract

Co-pyroclastic density current (co-PDC) plumes form as a mixture of fine-grained (< 90 μm) particles and hot gas loft from the top of pyroclastic density currents. Such plumes can rise tens of kilometres high and inject substantial volumes of fine ash into the atmosphere, with significant implications for airspace disruption and populations, livestock and agriculture in downwind areas. Co-PDC deposits have a remarkably consistent grain size that remains constant with distance from source, regardless of eruption style, highlighting the complex sedimentation mechanisms that control deposition of co-PDC ash due to its fine grain size. Observations and numerical simulations of co-PDC onset emphasize the role played by the dynamics of PDCs in the development of co-PDC columns and plumes. The key differences between co-PDC and vent-derived plume source conditions and dispersion dynamics have important implications for application of remote sensing and numerical modelling methods.

2. Introduction

A critical requirement in assessing volcanic ash hazard and quantifying related risk is accurate identification and characterization of sources of atmospheric ash (Rose and Durant, 2009; 2011). Ash injection and dispersion in the atmosphere during explosive eruptions is primarily associated with the formation of buoyant convective columns above volcanic vents (e.g. Bonadonna and Phillips 2003; Bursik 2001; Carey and Sparks 1986; Sparks 1986). In this context, a mixture of particles and gas is ejected from the conduit in a high velocity jet following fragmentation of magma ascending from depth in the conduit (Figure 1A). Convective plumes can also form from propagating pyroclastic density currents (PDCs).

PDCs are dry mixtures of gas, particles and entrained air that travel as fast moving density currents away from the eruptive vent (Figure 1B). While spreading, PDCs can generate secondary plumes by buoyant rise of hot gas and fine-grained material. Such plumes, here entitled 'co-pyroclastic density current plumes' (co-PDC plumes, also described as co-ignimbrite plumes and Phoenix clouds in the literature, e.g. Rosi et al. 2006; Sigurdsson and Carey 1989; Sparks and Walker 1977; Walker 1972) differ from vent-derived plumes in three principal ways (Figure 1B): 1) they are not characterised by a jet region at their base, 2) they initiate by buoyancy reversal of the material transported in the PDCs, and 3) they have a large source area.

PDCs occur frequently during explosive eruptions, and can be associated with years to decades-long low-level eruptive activities, including dome and lava flow-forming eruptions, as demonstrated by the recent activity at Soufriere Hills (Montserrat), Sinabung (Indonesia), Santiaguito (Guatemala), and Colima (Mexico). Observations of PDC emplacement, as well as analysis of pyroclastic deposits from recent and past eruptions, have shown that co-PDC plumes are associated with the entire size spectrum of PDCs, from hot rock falls and small volume PDCs (e.g. Bonadonna et al. 2002a; Calder et al. 2002; Eychenne et al. 2012), to massive expanded pumice and ash flows (e.g. Sparks and Huang 1980; Sparks and Walker 1977). Co-PDC plumes can rise through the atmosphere to altitudes of tens of kilometres, as illustrated by those formed during the May 18, 1980 Mount St. Helens and June 15, 1991 Pinatubo eruptions, which attained maximum heights of 30 km a.s.l (Holasek et al. 1996; Sparks et al. 1986). In fact, the Mount St. Helens co-PDC plume reached a greater height than the vent-derived plumes formed during the subsequent Plinian phase (Criswell 1987; Moore and Rice 1984). When co-PDC contributions have been distinguished from vent-derived tephra in fallout deposits, based on detailed studies of stratigraphy, grain size and componentry, co-PDC plumes have been shown to be capable of dispersing enormous volumes of fine-grained ash over entire continents (Pyle et al. 2006; Rose and Chesner 1987). For example, the large magnitude ignimbrite-forming Youngest Toba Tuff (Indonesia) and Minoan (Santorini) eruptions deposited more than 700 km^3 and 38 km^3 of co-PDC ash, respectively (Rose and Chesner 1987; Sigurdsson et al. 1990). Co-PDC ash represents ~ 60 vol% of the fallout deposit from the ignimbrite-forming Campanian eruption (Engwell et al. 2014), and up to 58 wt% of the fallout deposit from the 2006 Subplinian eruption of Tungurahua (Eychenne et al. 2012). Co-PDC plumes can thus contribute a significant proportion of the distal ash associated with very large, as well as intermediate sized, explosive eruptions.

These examples show that co-PDC plumes represent a substantial and recurring source of atmospheric ash during explosive eruptions, and constitute a significant and widespread hazard. Volcanic ash impacts communities on the ground by destroying crops and livestock, affecting infrastructure and causing health problems in humans. At Montserrat, the respiratory health hazards of co-PDC ash has been particularly important, due to the fine grain size and abundance of crystalline silicate phases (Baxter et al. 1999; Horwell and Baxter 2006; Horwell et al. 2001). In addition, the fine-grained nature of the ash allows it to remain suspended in the atmosphere for many days (Bonadonna et al. 2002a, 2002b; Rose and Chesner 1987), posing substantial risk for aviation (Gislason et al. 2011; Kueppers et al. 2014). Co-PDC plumes can also impact the global environment, by contributing substantially to climate forcing by injection of aerosols, and specifically sulphurous phases, into the atmosphere, with implications for climate many years after eruption (Guevara-Murua et al. 2014; Oppenheimer 2002).

There are a number of fundamental differences between co-PDC and vent-derived plumes in terms of, for example, grain size of the particulate load, particle concentration and ascent velocities (e.g. Bonadonna et al. 2002a; 2002b; Sparks 1976; Sparks et al. 1997;

Walker 1972). Distinguishing between the two plume types is therefore essential for hazard assessment, and proved crucial for investigating eruption dynamics during the 1991 Pinatubo eruption (Koyaguchi and Tokuno 1993) and for plume dispersion modelling at Montserrat (Bonadonna et al. 2002b). Accounting for co-PDC plumes when assessing hazard and risk related to volcanic ash dispersion requires comprehension of the specific processes controlling co-PDC plume formation, their injection into the atmosphere, and transport and sedimentation of co-PDC ash.

Accurate ash hazard assessment requires the integration of information from PDC, co-PDC and mixed fallout deposits (i.e. those that include both a co-PDC and a vent-derived contribution), with findings from analogue experiments in the laboratory and numerical simulations of PDC liftoff and formation of co-PDC columns. In this chapter, we review published data related to co-PDC plume formation, dispersion and sedimentation. In the following sections, we present an overview of dynamics and occurrences of co-PDC plumes and summarise observations from co-PDC plume-forming eruptions that encompass a range of eruption styles. Next, we summarize co-PDC deposit characteristics - specifically geometry, grain size and componentry - to highlight key spatial trends and provide insights for co-PDC plume formation, dispersion and sedimentation. We also summarise proposed theoretical models for co-PDC plume formation and insights gained from numerical modelling of co-PDC column development from propagating PDCs. Finally, we discuss appropriate considerations required for monitoring dispersion of co-PDC plumes using satellite infrared remote sensing methods, and for modelling co-PDC plume injection, dispersion and sedimentation processes.

In the following, the term "fallout deposits" refers to mixed deposits including tephra from both vent-derived and co-PDC plumes. We use the term "vent" to refer to the eruptive crater of a volcano, while "source" refers to the location of co-PDC plume liftoff. The term "proximal" describes the areas affected by column dynamics and PDC emplacement, "distal" corresponds to all distances at which deposit thickness is less than a few centimetres to a few millimetres depending on the eruption magnitude, and "medial" refers to all intermediate distances.

3. Overview

Co-PDC plumes develop from propagating PDCs, and thus do not have their source centred on volcanic vents (Figure 1B). These plumes form as particles sediment from the base of propagating currents, and air is entrained at the top (e.g. Andrews and Manga 2011; 2012; Bursik and Woods 1996; Sparks et al. 1997). The entrained air is heated by the particles, and expands. The combination of sedimentation and entrainment causes the density of the upper portions of PDCs to decrease below that of the surrounding atmosphere. This density decrease leads to a buoyancy reversal (Figure 1B; Bursik and Woods 1996; Woods and Wohletz 1991) and the formation of buoyant plumes. Buoyancy reversal can be enhanced by interaction of PDCs with topography, which favours sedimentation and air entrainment within the current (Andrews and Manga 2011; 2012). Co-PDC plumes ascend in the same manner as vent-derived plumes (Figure 1A), reach the level of neutral buoyancy and spread laterally by a combination of buoyant forces and atmospheric processes (Bonadonna and Phillips, 2003; Bursik et al. 1992a; 1992b; Sparks et al. 1986; Sparks et al. 1992). Formation of PDCs, vent-derived and co-PDC plumes can occur simultaneously during explosive eruptions, and even during a single eruptive event. Therefore, several sources may contribute to atmospheric ash injection during an explosive eruption, leading to complex mixed plumes and fallout deposits.

3.1. Ignimbrite-forming eruptions

The term ignimbrite refers to a voluminous PDC deposit formed by a very large eruption. The phenomena of co-PDC plumes was first highlighted in the context of ignimbrite-forming eruptions, where a distinct lack of fine-grained ash, and an enrichment in crystals in the matrix of the ignimbrite deposits, was used to suggest that gas and ash rich plumes lofted from the top of currents during their emplacement (Hay 1959; Lipman 1967; Sparks and Walker 1977; Walker 1972). Ignimbrite-forming eruptions typically have a magnitude M > 6.5 (on the scale from Pyle (1995) where M = $\log_{10}$(erupted mass, kg) - 7), and produce mixed fallout deposits which range from a few to thousands of km^3 in DRE (Dense Rock Equivalent) volume (Table 1) and disperse several thousands of kilometres away from source (Pyle et al. 2006; Rose and Chesner 1987). Such large eruptions have not occurred during historical times, and their eruption processes are therefore inferred by analysis of resultant deposits. This reveals that ignimbrite-forming eruptions typically initiate with development of vent-derived plumes, followed by or synchronous with extensive PDC propagation blanketing the topography (Branney and Kokelaar 1997; Sparks et al. 1973; Sparks and Wilson 1976). During emplacement of the PDCs, co-PDC plumes loft from the entire extent of the current, have source radii on the order of tens to hundreds of kilometres, and reach altitudes of several tens of kilometres (Costa et al. 2012; Woods and Wohletz 1991).

3.2. Plinian eruptions

PDCs are common during Plinian eruptions, often forming by collapse of the vent-derived column. Several historic eruptions have provided detailed observations of co-PDC plume formation and dispersion. The Plinian eruption of Mount Pinatubo in the Philippines on June 15, 1991, was the second largest eruption of the 20th Century, and produced both

Plinian and co-PDC plumes (Holasek et al. 1996; Koyaguchi and Tokuno 1993), leading to a mixed fallout deposit covering an area of ~4×10^5 km^2 with a DRE volume of 2.5 km^3 (Wiesner et al. 2004; Table 1). The voluminous pumice flows generated (2.1 - 3.3 km^3 in DRE volume) overflowed topography to about 10 km away from the vent and were channel-confined for the rest of their runout distances (Rosi et al. 2001; Scott et al. 1996). A PDC travelling in a valley to 16 km from the vent produced a co-PDC plume clearly identifiable from the ground and on satellite images (Holasek et al. 1996). The plume lofted from the entire length of the PDC as an elongate sheet-like column, and showed notable variation in diameter with height, with a narrowing directly above the PDC and a sudden increase of diameter between 500 m and 1 km from the ground (Figure 2A). This co-PDC plume rose to a height of 20.5 km and dispersed at altitudes 1.5 - 2 km lower (Holasek et al. 1996).

Lateral blasts, which are impulsive directed explosions of a part of a volcano due to sudden decompression of cryptodomes, generate extensive PDCs associated with efficient co-PDC plume formation (Druitt 1992). Perhaps the most famous example of co-PDC plume formation is that associated with the May 18th 1980 eruption of Mount St. Helens, U.S. (Table 1, Figure 2B). A devastating PDC generated by a blast travelled to 15 km from source and blanketed an area of ~ 600 km^2 to the north of the volcano in less than 6 minutes (Druitt 1992; Hoblitt et al. 1981; Moore and Sisson 1981). As the current interacted with topography, multiple plumes ascended from the PDC at velocities between 25 and 70 m/s, and rose 6 to 8 km-high (Hoblitt 2000; Moore and Rice 1984; Sparks et al. 1986). The final plume (Figure 2B) lofted from the entire area covered by the PDC and had a strong horizontal velocity component, presumably inherited from the northward directional energy of the blast (Eychenne et al. 2015). The plume was characterized by ascent velocities of ~ 110 m/s and a maximum height of 35 km (Holasek and Self 1995; Sparks et al. 1986). It spread at an altitude of 10 to 12 km (Eychenne et al. 2015), controlled by gravitational processes for the first 100 km from source (Bursik et al. 1992a).

3.3. Intermediate size eruptions

Vulcanian and Subplinian eruptions, with magnitudes typically smaller than 5 (Table 1), are characterized by unsteady vent-derived columns leading to formation of small volume (a few tens of km^3 in DRE volume), channelized, pumice and scoria flows (e.g. Bonadonna et al. 2002a; Calder et al. 1997; Cole et al. 2014; Hoblitt 1986; Stinton et al. 2014). Coeval formation of both vent-derived and co-PDC plume is common during such eruptions. Pumice flows generated by the short-lived, pulsating eruption of Mount St. Helens on August 7, 1980 (Hoblitt 1986) produced co-PDC plumes with maximum vertical velocities of 5 to 13 m/s, despite initial velocities of only 1 to 2 m/s (Calder et al. 1997). Interaction of the pumice flows with topographic changes, either breaks in slope or bends in the channel, triggered formation of multiple individual plumes along the length of a single flow (Hoblitt 1986). With initial radii of ~ 50 to 200 m, the plumes merged during ascent and attained heights of 400 to 800 m (Calder et al. 1997).

3.4. Dome Collapse events

Co-PDC plumes frequently rise from small volume, channel-constrained, PDCs generated by dome (e.g. Bonadonna et al. 2002a; Calder et al. 2002; Cole et al. 1998; Miyabuchi 1999; Stinton et al. 2014; Watanabe et al. 1999; Woods and Kienle 1994) and lava flow collapses (e.g. Evans et al. 2009). These collapses occur as viscous magma that has been extruded at the vent becomes gravitationally unstable, producing PDCs without development of an eruptive column at the vent. These PDCs often comprise a dilute upper part forming a cloud of hot gas and ash, which can detach from the denser part of the current on interaction with topography (Watanabe et al. 1999). Discrete plumes develop sequentially from this dilute upper cloud and rise as a line of plumes that later coalesce during ascent, as observed during dome collapse activity at Soufriere Hills, Montserrat, in 1997 (Figure 2C; Bonadonna et al. 2002a; Calder et al. 2002; Cole et al. 2002). At Montserrat, the resultant co-PDC plumes occasionally detached from the source PDCs, and rose to heights of a few hundred metres to 15 km before dispersing many kilometres downwind. Co-PDC plumes associated with dome collapse events at Mount Redoubt, Alaska, in 1990 (Figure 2D) reached heights of 12 km, had ascent velocities on the order of 10 m/s (Woods and Kienle 1996), and dispersed ash 100 to 200 km from vent (Scott and McGimsey 1994).

3.5. Summary

Observations made during historical eruptions of various styles and scales provide critical information about the dynamics of co-PDC plumes. Coeval formation of both vent-derived and co-PDC plumes during a single event is common. Co-PDC plumes can either form as multiple discrete plumes lofting from the top of channel-constrained PDCs before coalescing at height to form a single plume, or as liftoff occurs from the entire extent of PDCs. Interaction of currents with topography changes enhances the development of co-PDC plumes.

The effective source area of co-PDC plumes is much larger than vent-derived columns (Figure 1), and is generally controlled by the width of the parent PDCs. Reported ascent velocities are variable, on the order of many tens to hundreds of m/s for large magnitude eruptions, and of ~ 10 m/s for smaller events. Maximum co-PDC plume heights can reach more than 30 km during large eruptions, while they are commonly on the order of hundreds of meters to a few kilometres during intermediate to small events. The examples of co-PDC plumes formed during Plinian events were not greatly affected by wind, and show significant differences between maximum and neutral buoyancy heights (Figure 1), similar to those observed in strong vent-derived plumes (Bonadonna and Phillips 2003). Initial intrusion of the plumes into the atmosphere occurred radially, regardless of wind direction (Bursik et al. 1992a; Holasek et al. 1996; Sparks et al. 1986; Woods and Kienle 1994), which implies that initial spreading velocities were greater than typical stratospheric wind speeds. Co-PDC plumes from smaller dome collapse, Vulcanian and Subplinian events are strongly affected by wind, showing a classic bent over shape (e.g. Calder et al. 1997) typically seen in wind-affected vent-derived plumes.

4. Characteristics of co-PDC deposits

In this section, the characteristics of co-PDC and mixed fallout deposits are described for eruptions where different co-PDC contributions have been inferred (Table 1).

4.1. Stratigraphy

Most pyroclastic deposits associated with large magnitude ignimbrite-forming eruptions can be described by a simplified stratigraphy, that includes a coarse-grained (10's cm to a few mm) Plinian vent-derived deposit at the base (e.g. Rosi et al. 1999; Paladio-Melosantos et al. 1996; Scott et al. 1996), that is overlain by PDC deposits of up to hundreds of metres thick in proximal locations, with runout distances on the order of many tens of kilometres, covering areas of many thousands of square kilometres and representing volumes up to hundreds of cubic kilometres (see Table 1 for examples and references). Co-PDC deposits were identified both overlying and inter-bedded within individual PDC units, and were described as fine grained (<125 μm) ash layers rich in glassy particles (Hay 1959; Sparks et al. 1973; Sparks and Walker 1977). Ubiquitous accretionary pellets (following the definition of Brown et al. 2012) have also been found in co-PDC layers (e.g. Brown and

Branney 2004). During ignimbrite-forming eruptions, proximal Plinian and co-PDC deposits may be eroded or buried during emplacement of PDCs and later eruptive episodes, such that an entire eruptive sequence is often not observable at a single outcrop. At distances beyond the reach of the PDCs, it is possible to identify fine-grained ash layers corresponding to co-PDC deposits directly overlying Plinian deposits (Figure 3; Engwell et al. 2014; Ninkovich et al. 1978; Sparks and Huang 1980; Wiesner et al. 1995). With increasing distance from source, as the grain size of the Plinian deposit fines, it becomes increasingly difficult to differentiate the two deposits, both in terms of their stratigraphy and grain size (Figure 3), and a single layer of ash is generally observed.

Pyroclastic deposits from PDC-forming, Plinian to Vulcanian eruptions are considerably smaller in extent and volume (see Table 1 for examples and references). In such examples, PDC deposits occur as multiple, often channelized, lobes and fans, producing stratigraphic sequences that vary significantly over spatial scales of a few tens of kilometres (Bernard et al. 2014; Brand et al. 2014; Charbonnier and Gertisser 2011; Druitt 1992; Hoblitt 1986). Distinct co-PDC ash layers with similar characteristics to those associated with ignimbrite deposits have been documented close to source on top of sequences of smaller PDC units (Cole et al. 2002; Criswell 1987; Eychenne et al. 2012; Kuntz et al. 1981; Miyabuchi 1999; Ritchie et al. 2002). These co-PDC deposits appear as structureless layers of fine ash (< 90 µm), millimetres to a few centimetres-thick, often bearing accretionary pellets (Eychenne et al. 2012; Ritchie et al. 2002; Watanabe et al. 1999). Beyond PDC runout distances, distinct co-PDC ash layers are not easily identifiable based on stratigraphy alone, due to coeval formation and interaction of vent-derived and co-PDC plumes, common during Vulcanian, Subplinian and Plinian eruptions (Bonadonna et al. 2002a; Di Muro et al. 2008; Eychenne et al. 2012). When vent-derived and co-PDC plumes form during the same eruptive episode, medial to distal fallout deposits occur as massive tephra beds, comprising a mixture of co-PDC and vent-derived material (Bonadonna et al. 2002a; Eychenne et al. 2012; 2015; Sarna-Wojcicki et al. 1981). An important signature of these unstratified mixed fallout deposits is their bimodal grain size distributions, which are further described in section 4.4. Dome collapse events, which lack vent-derived plumes, offer the best opportunities to observe and document co-PDC ash sheets to distal locations (Bonadonna et al. 2002a; 2002b; Watanabe et al. 1999).

4.2. Geometry and volume of co-PDC and mixed fallout deposits

Co-PDC deposits formed during dome collapse events (Bonadonna et al. 2002a; Watanabe et al. 1999) have elongate and rather broad proximal regions located away from the eruptive vent (Figure 4). This reflects the geometry of the co-PDC columns as they rise from the length of the channelized PDC (Bonadonna et al. 2002a; Calder et al. 1997; Cole et al. 2002), controlled by the orientation of the constraining drainage channel. Despite these controls however, the proximal footprint of co-PDC deposits appears to depend primarily on wind, with isopachs displaced, and sometimes even detached, from the area of PDC emplacement in the downwind direction (Figure 4). In medial and distal areas, these proximal effects become insignificant, and deposit geometries and axes are ultimately controlled by the atmospheric winds (Figure 4A, B and C). A number of co-PDC deposits show secondary maxima in thickness and mass at distance downwind from the vent (Figure 4D; Bonadonna et al. 2002a; Watanabe et al. 1999), a feature also observed in some mixed fallout deposits (Figure 5A; Eychenne et al. 2015).

In examples of mixed fallout deposits where the co-PDC and vent-derived contributions were distinguished (based on componentry and grain size), enrichment in co-PDC ash has been shown to strongly impact the footprint of the mixed fallout deposit. Contribution of co-PDC plumes rising from large source areas, such as those that form in association with emplacement of PDCs that are not controlled by topography (Table 1), can lead to mixed fallout deposits with broad proximal geometries (Figure 5A; Eychenne et al. 2015). In addition, PDCs derived from lateral blast events can produce co-PDC plumes with a strong horizontal component, leading to the up- and/or cross-wind displacement of the mixed fallout deposit (Figure 5A; Eychenne et al. 2015). Localized enrichment in co-PDC ash, which can occur downwind of a topographic barrier perpendicular to the PDCs propagation direction, can cause an over-thickening of the mixed fallout deposit leading to complex deposit shapes (Figure 5B; Eychenne et al. 2012).

Volumes of co-PDC deposits formed during dome collapse events are typically small, ranging from 2×10^{-5} to 9×10^{-4} km^3 (Table 1), and accounting for 4 to 30% of the volume of associated PDCs (Bonadonna et al. 2002a; Watanabe et al. 1999). Despite such small volumes, the fine-grained nature of co-PDC ash allows its dispersion and deposition over much larger areas than would be expected for a vent-derived eruption of the same magnitude. Co-PDC deposits associated with large magnitude ignimbrite-forming eruptions have been shown to have similar volumes to deposits from vent-derived plumes formed during the same eruption (Table 1 and references therein). Their volumes range from 6 km^3 to 2000 km^3. In some examples, inferred co-PDC volume is considerably larger than the volume of material dispersed by vent-derived plumes (Table 1).

4.3. Componentry of co-PDC deposits

The matrix of ignimbrite deposits is typically enriched in phenocrysts compared to scoriae or pumice from the same eruption (Hay 1959; Lipman 1967; Sparks 1976; Walker 1972). This observation suggests that much of the vitric (glassy) material is not deposited by the PDCs and must instead settle as co-PDC ash (Hay 1959; Sparks et al. 1973; Sparks and Walker 1977; Walker 1972). Some crystals in the PDC matrix, however, originate from fragmentation or comminution of accidental and accessory material (Lipman 1967). Therefore, the extent to which the degree of crystal enrichment in PDCs can be used to infer the volume of co-PDC deposits is limited.

In fact, co-PDC ash layers are not solely composed of vitric glass; they may also contain a non-negligible proportion of crystals (3 to 14 wt% in grain size fractions < 2 mm) and non-juvenile material (1 to 12 wt% in grain size fractions < 2 mm, Sparks 1975; 1976; Sparks and Walker 1977). In co-PDC deposits formed during dome collapse events, where the juvenile material is microlite-rich, crystals can constitute up to 50 wt% of material coarser than 63 μm, and up to 70 wt% of the finer material (Bonadonna et al. 2002a; Watanabe et al. 1999). In such samples, micro-crystalline silicate phases appear concentrated in co-PDC deposits with respect to the matrix of the PDCs, especially in the sub-10 μm fractions (Baxter et al. 1999; Horwell et al. 2001). Finally, co-PDC plumes associated with PDCs with a high content of non-juvenile material, such as blasts (which are accompanied by the collapse of volcanoes' flanks), can settle ash dominated by lithic material (Eychenne et al. 2015).

These data show that crystals and various types of non-juvenile particles can constitute a considerable proportion of co-PDC deposits, suggesting that co-PDC plumes do not entrain solely low density material (such as glass shards). The componentry of co-PDC deposits is highly variable from one eruption to another, and appears to be controlled by the nature of the source material and fractionation processes occurring during PDC propagation, and not only by the processes controlling the formation of the co-PDC plumes, which will be discussed further later.

4.4. Grain size of co-PDC and mixed fallout deposits

The grain size of co-PDC deposits is characterized by a unique signature, which has proved a critical tool for distinguishing co-PDC from vent-derived contributions in mixed fallout deposits.

4.4.1. Methods for analysing particle size distributions of fallout deposits

Because of the fine-grained nature of co-PDC deposits (see section 4.4.2), their particle size distributions (PSD) cannot be resolved by traditional sieving methods, and a number of more complex techniques have been employed for collection of the grain size data compiled here (Table 1). The most common method in modern studies is laser diffraction (e.g. Di Muro et al. 2008; Eychenne et al. 2012; Miyabuchi 1999), which determines the size distribution of a suspension of particles by measuring the light intensity of a laser beam at low scattering angles passing through the suspension. This method applies different light scattering theories (e.g. Mie, Fraunhofer approximation), which require an assumption regarding the optical parameters (refractive index, light absorption) and shape of the particles (often approximated to spheres). Another widely used technique is electrozone sensing (e.g. Bonadonna et al. 2002a; Brazier et al. 1982; Sparks and Huang 1980), whereby particles suspended in an electrically conductive fluid are counted, and their size is inferred by measuring the electrical resistivity of the fluid while individual particles are forced through a small opening. After calibration with known size standards, this technique gives repeatable results for non-spherical particles. Finally, a number of studies have measured the sedimentation rate of individual particles falling through a liquid of known density, with particle size estimated assuming a settling velocity law (e.g. Watanabe et al. 1999; Wiesner et al. 2004). One limitation of this method arises from difficulties in obtaining adequate experimental conditions to ensure individual settling of particles finer than 63 μm, and the lack of constraints on the flow regime controlling their settling. In addition, assumptions concerning particle shape (generally spherical) and density (variability in material is often not considered) are required to compute the settling velocity law. All of these methods require some form of approximation, which do not encompass the complexity of volcanic ash (see Cashman and Rust's chapter), and therefore caution is advised when comparing PSDs determined by different techniques.

Commonly grain size analyses of mixed fallout deposits (including both vent-derived tephra and co-PDC ash) is conducted by combining sieve data (for material coarser than 90 μm) with one of the methods described above (for measuring material finer than 90 μm) (Table 1). To obtain a complete distribution, the two resultant datasets are merged by: 1) converting the PSDs obtained by laser and electrozone techniques from volume to mass, assuming a value of particle density, and 2) calibrating sieve data with the method used for measuring the fine grains, by overlapping the measurements in a given size range (Eychenne et al. 2012; Wiesner et al. 2004).

The PSDs obtained by these methods are described by a probability density function using the Krumbian phi scale ($\Phi = -\log_2(d/d0)$, where d is the diameter of the particle and $d0$ is a reference diameter equal to 1 mm), widely adopted in geology (Folk and Ward 1957). PSDs from fallout deposits can be polymodal and rarely follow a mathematical function. In early studies, distinct peaks in polymodal PDSs were separated into individual subpopulations by hand (Brazier et al. 1983). More sophisticated methods to deconvolve polymodal PSDs assume that they consist of a combination of log-normal subpopulations (Wohletz et al. 1989). Here, we have deconvolved polymodal distributions (where not processed in the original studies, see Table 1) by fitting identifiable modes of the raw distributions without assuming that they follow a specific mathematical function. We use algorithms based on the versatile Weibull function, which can reproduce the shape of many probability density functions, and thus allows extraction of non-lognormal subpopulations

(Caballero et al. 2014; Eychenne et al. 2012; 2015). Unimodal distributions and deconvolved subpopulations are described using median diameter (Md) and sorting (σ) parameters, determined following the graphical method of Inman (1952).

4.4.2. *Grain size characteristics of co-PDC and mixed fallout deposits*

Despite differences in geological context (chemistry of the magma, crystal content, etc.) and eruptive dynamics (eruption style, magnitude, PDC type and trigger), the co-PDC deposits have very similar grain size distributions (Figure 6, Table 1). Generally unimodal, they have a median diameter (Md) between 3.5 and 6 Φ (90 and 15.6 microns) which does not vary with distance from source (Figure 6). These consistent co-PDC grain size characteristics suggest that processes controlling the entrainment of particles in co-PDC columns are fundamentally size-selective, with particles coarser than about 90 µm not preferentially lofted.

Both large and intermediate magnitude PDC-forming eruptions for which grain size analyses of the fallout deposit have been published are listed in Table 1. Most of these fallout deposits are unstratified over the area sampled, and are assumed to contain both co-PDC and vent-derived ash. The other deposits comprise a coarse lower (10's cm - mm) and fine upper (< 125 microns) unit in proximal locations, and a massive ash layer at greater distances (Figure 3). The grain size data presented here correspond to the vertically averaged deposit (where grain size of individual units are weighted according to the units thickness). All of the fallout deposits have bimodal particle size distributions at individual locations in the deposit, regardless of eruption magnitude or style. The fallout deposits documented across great distances change from bimodal to unimodal distributions in distal and off-axis regions (Figure 6).

The coarse and fine subpopulations retrieved by deconvolution of the bimodal PSDs display a consistent spatial pattern. The coarse subpopulation Md decreases with distance from vent, while the Md of the fine subpopulations is quasi-constant over the whole extent of the deposit (Figure 6A). Distributions are unimodal at distances where the coarse subpopulation Md converges towards the value of the fine subpopulation Md. The decay rate of the coarse subpopulation Md with distance from vent varies from one eruption to another, with the high magnitude eruptions (Plinian and ignimbrite-forming) showing a slower decay rate than low magnitude events (Vulcanian and Subplinian) (Figure 6). Only the fine subpopulation Md from the Vulcanian and Subplinian eruptions decrease slightly in size with distance from vent (Figure 6). The grain size of the fine subpopulation Md in bimodal deposits is similar to those of the co-PDC grain size distributions, ranging from 63 to 30 µm (Figure 6).

4.4.3. *Origin of the bimodality in mixed fallout deposits*

The spatial variation of the grain size subpopulations in the bimodal distributions of mixed fallout deposits have been linked to co-PDC contribution in several studies using different lines of evidence (e.g. Di Muro et al. 2008; Eychenne et al. 2012; Sparks and Huang 1980). The spatial variation of stratification observed in large magnitude eruptions (Engwell et al. 2014; Sparks et al. 1984; Wiesner et al. 2004) provides evidence for contemporary deposition from both co-PDC and vent-derived plumes. The coarse and fine proximal units are inferred to derive from a vent-derived Plinian and co-PDC plumes, respectively (Engwell et al. 2014; Sparks et al. 1984; Sparks and Huang 1980). At intermediate distances, contribution from co-PDC and vent-derived plumes cannot be distinguished stratigraphically, and a massive bimodal ash layer resulting from sedimentation of both plume types is evident (Figure 3; Engwell et al. 2014; Sparks et al. 1984; Sparks and Huang 1980). At greater distances, the bimodality vanishes, and the ash deposit has a unimodal PSD, often skewed towards the fine grain sizes (Figure 3; Engwell et al. 2014). This depositional pattern suggests that mixing of the two source contributions produces bimodality in these fallout deposits to distances where the vent-derived plume is depleted in large particles, at which point the remaining vent-derived ash is of a similar size to the co-PDC ash (Engwell et al. 2014). This mechanism can also be invoked to explain the convergence of the coarse and fine subpopulation Md trends towards the unimodal distributions (Figure 6).

Componentry changes were compared to the spatial variations of the proportion of fine and coarse subpopulations in the mixed fallout deposit from the 1980 Mount St. Helens Plinian eruption. Accounting for the complex syn-eruptive wind field, this comparison has shown that the consistent fine subpopulation was deposited by a co-PDC plume resulting from a blast-PDC, while the coarse subpopulation was deposited by a vent-derived plume formed later during the eruptive sequence (Eychenne et al. 2015).

5. Controls on co-PDC plume formation

The formation of co-PDC plumes is intimately related to processes occurring within the parent PDC. The consistent co-PDC grain size characteristics described above (Figure 6) suggests that processes controlling the entrainment of particles in co-PDC columns allow the preferential lofting of particles finer than about 90 μm. A number of mechanisms have been identified as leading to the formation of co-PDC plumes. Fine particles are mobilised from the dense basal portion of the flows towards the turbulent upper portions, by escaping gas, in a process called elutriation. The source of this gas may be internal - continuing release of magmatic gas from hot juvenile material (Sparks 1978) - or external to the current - from incineration of vegetation, or formation of steam on interaction with ice (Woods and Kienle

1994) or water bodies (Moore and Rice 1984; Sigurdsson and Carey 1989). When gas velocities are greater than particle terminal velocity, these particles elutriate from the dense basal flow into the overriding turbulent suspension. As the hot current propagates beneath the effectively stagnant air, a turbulent shear boundary forms, aiding entrainment of hot particles from the main body of the flow as ambient air is forced over the top (Denlinger 1987). Finally, buoyant lift off of the whole current is proposed to occur during emplacement of large PDCs as sedimentation and ambient air entrainment lowers the density of the flow to less than that of the ambient (Sparks et al. 1986; Sparks et al. 1997).

5.1. Source conditions

Detachment and rise of the upper turbulent portion of a propagating current occurs when its density becomes equal to that of the surrounding atmosphere, a process called buoyancy reversal. Gas mass fractions of 30 - 60 % are required for the mixture to reach an equivalent density to the atmosphere (Woods and Wohletz 1991). Such fractions are considerably greater than the gas mass fraction of the mixture emitted at vent (1 – 5 %; Sparks et al. 1986; Wilson et al. 1980). The density of the flow decreases by a combination of particle sedimentation, and the entrainment, heating and thermal expansion of ambient air. These processes have been thoroughly investigated using analogue experiments, whereby a dense sediment rich fluid is injected into a sloped or flat tank of less dense saline fluid (e.g. Carey et al. 1988; Huppert et al. 1986; Sparks et al. 1993; Woods and Bursik 1994; Woods and Caulfield 1992). These experiments highlight the role of entrainment in lowering current density. They also show that increasing slope enables greater entrainment, related to increased shear mixing and consequently buoyancy reversal sooner than on shallow slopes (Woods and Bursik 1994). However, thermal expansion of entrained fluid, a key process for the formation of co-PDC plumes, is not accounted for in these experiments. Experiments where heated mixtures of talc (~ 22 microns in diameter) were fed into a tank to generate turbulent dilute mixtures highlight the importance of this process, and show that mass fractionation into co-PDC plumes scales with the temperature of the current (Andrews and Manga 2011; 2012).

Buoyancy reversal can also occur as PDCs interact with topography, resulting in the formation of discrete co-PDC plumes along the PDC runout as described in section 3, due to enhanced mixing locally and subsequent thermal expansion of air, causing strong fines depletion in PDC deposits (Branney and Kokelaar 2002; Druitt 1998; Sparks et al. 1997). Detailed field studies of blast-derived PDC deposits show that the current becomes progressively more dilute as it propagates, with increased sedimentation ahead of topographic highs (Druitt 1992; Hoblitt et al. 1981; Moore and Sisson 1981). Enhanced mixing and entrainment of ambient air also accompany hydraulic jumps, which occur as PDCs encounter a sudden change in slope causing an increase in flow thickness and a decrease in flow velocity (Branney and Kokelaar 2002; Freundt and Schmincke 1985; Levine and Keiffer 1991).

In large eruptions, buoyancy reversal can affect the entire current resulting in buoyant lofting from the entire PDC extent to form giant plumes (Sparks et al. 1986; 1997). The May 18, 1980 Mount St Helens blast-related co-PDC plume (section 3.2) is inferred to have formed by such buoyant lofting (Figure 2B; Moore and Rice 1984; Sparks et al. 1986). Observations of horizontal velocities of 100 m/s close to the final extent of the PDC (Moore and Rice 1984) imply high mass flux rates within the flow at the time of lofting and indicate rapid transition from horizontal to vertical momentum as a result of buoyancy reversal.

5.2. Insights from numerical models for column dynamics

Numerical modelling of column dynamics is essential to identify inputs required for atmospheric dispersal models. Numerical modelling of co-PDC plume formation and rise has typically involved the modification of models normally applied to vent-derived plumes (e.g. Woods and Wohletz 1991). Co-PDC plumes have been simulated using steady-state co-PDC models (Calder et al. 1997; Woods and Wohletz 1991), by buoyant thermal theory (Calder et al. 1997; Woods and Kienle 1994), and using multiple phase (e.g. gas and particulate) complex numerical models (Dobran and Neri 1993; Herzog and Graf 2010; Neri and Dobran 1994) .

In one-dimensional steady state and buoyant models, the rising mixture is assumed to be just buoyant relative to the atmosphere, well mixed and in thermal equilibrium (Woods and Kienle 1994; Woods and Wohletz 1991). It is also generally hypothesized that the mixture has little to no initial momentum (vertical velocity in the range 0.1 – 10 m/s), based on observations of small volume discrete co-PDC plumes associated with intermediate size eruptions (Calder et al. 1997). Yet, as stated above, much greater velocities have been observed during large eruptions where buoyant lofting occurs from the whole PDC extent (Moore and Rice 1984).

The application of steady state models (Calder et al. 1997; Woods and Wohletz 1991) requires the assumption that the current provides a constant source of material over time scales longer than the ascent time of the co-PDC plume. Equations for mass, momentum and thermal conservation are solved with height taking both entrainment of ambient air and particle sedimentation into account. Characterisation of entrainment is key for accurate modelling of volcanic plumes, and is specified using an entrainment coefficient in one-dimensional models. Entrainment rates are particularly poorly defined for co-PDC plumes, where the large initial radius means that entrained air may not mix completely within the column (Calder et al. 1997). Two entrainment assumptions have been applied when modelling co-PDC plumes: 1) constant entrainment with height (Woods and Wohletz 1991), and 2) variable entrainment with height (Calder et al. 1997) with reduced entrainment near the ground, allowing the small scale of turbulent eddies relative to plume radius to be taken into account (Calder et al. 1997; Sparks et al 1997). Comparison of results obtained using these different assumptions shows differences in velocity at the base of the plumes, but no significant difference in the final plume height (Sparks et al. 1997). With the steady state model (Woods and Wohletz 1991), strong contraction in plume radius is observed immediately after lofting (Figure 7). Such a phenomena has been observed in the formation of large co-PDC plumes (section 3.2 and Figure 2D). The contraction is related to the decrease in plume density relative to the ambient (Figure 7). As ambient air is entrained and expands, the plume becomes buoyant and accelerates upwards (Figure 7), resulting in an increase in mass flux per unit area with height which is faster than the rate of addition of mass by entrainment. As a consequence, the plume radius decreases (Figure 7) to conserve mass (Woods and Wohletz 1991).

A discrete thermal model (Woods and Kienle 1994) was proposed following observations of co-PDC plumes formed during dome collapse events. The model assumes hot material is elutriated on short timescales compared to the ascent time in the atmosphere, and rises as a discrete spherical hot cloud. The model predicts that the height of the co-PDC plume is dependent on the initial mass, temperature and velocity of the cloud. While trends in velocity and density with height are similar to the steady state example (Figure 7), results do not show the same radial contraction, and instead radius increases linearly with height (Figure 7). In both models, the maximum plume height is calculated as the height at which the vertical velocity is zero. Application of the steady state and discrete thermal models in 1D to small volume co-PDC plumes from intermediate size eruptions show that in reality neither model completely describes plume ascent dynamics, but that the solution lies somewhere between these end members (Calder et al. 1997).

A two-dimensional axisymmetric two-phase numerical model has also been used to investigate the processes associated with the formation and rise of co-PDC plumes (Dobran and Neri 1993; Neri and Dobran 1994). This model accounts for thermal disequilibrium between the particles and gas, and for particle-particle interaction. The production of co-PDC plumes appears to be dependent on the fine-grained particles in the mixture, which follow the gas phase as it separates from the current. Model results reproduce the formation of multiple buoyant clouds above propagating currents, resulting in a substantial decrease in the spreading rate of the parent PDCs. This was also noted in hot granular experiments (Andrews and Manga 2012), where plume liftoff is seen to inhibit further spreading of the parent current. The modelled co-PDC plumes ascend rapidly, entraining large volumes of air. Strong contraction in plume radius immediately after lofting is also observed (Dobran and Neri 1993), as seen in results from the steady state model (Figure 7).

Finally, application of three-dimensional multiphase flow models (Herzog and Graf 2010) to simulate co-PDC plume rise highlights the importance of multiple discrete source locations on controlling plume dynamics, resulting in reduced neutral buoyancy heights compared to vent-derived examples. A key result is the difference in predicted neutral and maximum heights of co-PDC plumes, which cannot be easily differentiated using one-dimensional models, and can be on the order of tens of kilometres (see section 3), an important consideration for applying dispersal models to co-PDC plumes.

6. Dispersion and sedimentation of co-PDC ash

6.1. Importance of enhanced sedimentation

The grain size compilation (Figure 6) reveals that the coarse subpopulation of mixed fallout deposits decreases in size with distance from vent. In comparison, co-PDC ash and the fine grain subpopulations from mixed fallout deposits (assumed mainly co-PDC in origin): 1) have a much finer median size (about 63 μm), 2) show no variation of grain size with distance, and more importantly 3) settle continuously from the source to distal locations. The coarse trend converges towards the fine trend with distance. The coarse trend is consistent with particle size fractionation in a laterally spreading volcanic plume due to sedimentation governed by individual particle settling in a turbulent to intermediate regime (Bonadonna et al. 1998; Bursik et al. 1992b; Durant et al. 2009; Fisher 1964; Sparks et al. 1992). The fine trend suggests that particles $<$ 63 μm in size continuously exit the plume during dispersion and that only the absolute amount of grains released, and thus the sedimentation rate, decreases with distance from source (as evidenced by the overall thinning of the deposits; Figures 4 and 5). This indicates that the fine particles do not settle following Stokes law as expected for grains of low Reynolds number whereby frictional forces control particle terminal velocity (i.e. settling in a laminar regime; Bonadonna et al. 1998). Stokes law predicts that particles smaller than 100 μm have a relatively long residence time in the atmosphere and only start settling several hours or days after eruption (Rose and Durant 2009), meaning that deposition would not begin until hundreds of kilometres from source (due to the advection of the plume by winds). Stokes law also predicts the deposits should display a decreasing grain size with distance (Bonadonna et al. 1998). The grain size characteristics in Figure 6 suggest that coarse and fine particles, dominantly from vent-derived and co-PDC plumes respectively, settle at similar distances from source and possibly at the same time (but not necessarily from the same height, e.g. Di Muro et al. 2008) despite their contrasting sizes; such a phenomena is not captured by settling theory for individual grains.

Different mechanisms of enhanced sedimentation can be invoked to explain sedimentation of fine particles closer to the vent than expected for individual particle settling, and local increase of sedimentation rates. Aggregates, formed by particle clustering or adhering to the surface of larger clasts due to wet or electrostatic forces (Brown et al. 2012; Rose and Durant 2011; Taddeucci et al. 2011; Van Eaton et al. 2012), are often observed in proximal fallout deposits. They are assumed to form in vent-derived columns and plume corners where particle interaction is more intense due to high particle concentrations (Brown et al. 2012; Van Eaton and Wilson 2013). Observations of accretionary pellets in proximal co-PDC deposits indicate that aggregation is relevant for co-PDC columns too (Bonadonna et al. 2002a; Eychenne et al. 2012; Watanabe et al. 1999). Water is known to play a crucial role in aggregate formation (Brown et al. 2012), and co-PDC plumes are likely to entrain more water than vent-derived plumes due to the interaction of the PDCs with water bodies (lake, rivers, glaciers, ocean, etc., e.g. Hoblitt 2000) and vegetation. A number of other processes could potentially contribute to continuous sedimentation of fine particles over great distances. One such process relates to entrainment of fine particles in the wake of settling coarser grains (Eychenne et al. 2015; Rose et al. 2008; Di Muro et al. 2008). This is particularly relevant in the context of synchronous co-PDC and vent-derived plume dispersion at different altitudes. The passage of large particles through a suspension of fine particles is likely and could produce the consistent trend in fines with distance seen in Figure 6. Another model is linked to the development of layers of fine-grained material at the base of spreading plumes (Carazzo and Jellinek 2012; 2013; Manzella et al. 2015), which periodically collapse due to gravitational instabilities. The development of these layers is favoured by interaction of particles of different sizes and a high content of fine grains (Carazzo and Jellinek 2013), and by growth of ash-bearing ice hydrometeors (Durant et al. 2009). Release of material driven by gravitational instabilities could explain the secondary maximum in thickness and mass observed in some co-PDC and mixed fallout deposits (Figures 4 and 5; Bonadonna et al. 2002a; Durant et al. 2009; Eychenne et al. 2015; Watanabe et al. 1999). Given the high concentration of fine ash in co-PDC plumes, sedimentation by gravitational instabilities may also explain the settling of these grains close to source.

6.2. Source parameters for numerical modelling of dispersion and sedimentation

Observations and simulations of co-PDC plumes (sections 3 and 5) consistently highlight the complexities of co-PDC source conditions relative to vent-derived plumes, with implications for numerical modelling of co-PDC ash dispersal. The initial plume radius is much larger or commonly described by multiple source areas making estimation of mass flux into the spreading plume problematic. During eruptions with synchronous vent and co-PDC activity, multiple plumes may be present in the atmosphere at different heights at the same time (e.g. Di Muro et al. 2008; Engwell et al. 2014; Eychenne et al. 2012; Rose et al. 2008). Specific attention must be paid to the co-PDC particle release height, as wind speeds and directions can vary drastically at different atmospheric levels, and therefore have a significant impact on model results (e.g. Bonadonna et al. 2002a; 2002b). Although co-PDC deposits formed from different types of eruptions share similar grain size trends (Figure 6), source radius and number of contributing discrete clouds varies with eruption. Critically, the total grain size distribution of the particulate material in co-PDC plumes is much finer than in vent-derived plumes (Bonadonna and Houghton 2005).

Intrusion of large co-PDC plumes into the atmosphere at neutral buoyancy occurs as a radially spreading gravity current (Holasek et al. 1996; Sparks et al. 1986; Woods and Kienle 1994). Buoyancy related processes can dominate plume dispersion for many hundreds of kilometres from source and have a great effect on downwind dispersion and sedimentation patterns (Baines and Sparks 2005). Advection-diffusion processes only become dominant at distance from source, dependent on the mass flux of the intruding plume (Pouget et al. 2013), and the strength of the wind. Numerical models commonly utilised in simulating ash dispersion assume that a mixture of material with defined grain size characteristics is released into the atmosphere from a point or line source, and dispersed by advection-diffusion following the dominant wind direction (e.g. Beckett et al. 2014; Bonadonna 2006; Folch et al. 2010). Such numerical applications have been applied to simulate dispersion from several co-PDC plumes (Bonadonna et al. 2002b; Costa et al. 2012; Folch et al. 2010; Johnston et al. 2012; Matthews et al. 2012). In a small number of examples, gravity current sedimentation models have been applied to co-PDC plumes, and have proved successful in inferring eruptive timescales and reproduce grain size trends (Kandlbauer et al. 2013). While the advection-diffusion models do not accurately describe near source plume intrusion dynamics, the gravity current models do not describe distal dispersion well and a combination of both processes is required to accurately reproduce deposit trends (Pouget et al. 2013). Neither model type is capable of accounting for the complex sedimentation processes key for description of co-PDC ash deposition (see section 6.1), which has a strong impact on predicted dispersion (paths and concentrations).

Results from numerical models are typically compared with actual deposit trends (specifically the mass per unit area at individual locations) in order to infer the source parameters of past eruptions, for example height of dispersion and eruption duration. By grouping vent-derived with co-PDC eruptive phases, large uncertainties may be incorporated when estimating eruptive source parameters. Volumes of co-PDC deposits can be significantly greater than those from vent-derived plumes in large magnitude eruptions (Pyle et al. 2006), with volumes the same order of magnitude of the parent PDCs (e.g. Scarpati et al. 2014; Sparks and Walker 1977). Such assumptions and simplifications in modelling co-PDC events may thus limit our understanding of dispersal processes significantly, not only producing inconsistencies in operational simulation of atmospheric ash dispersion, but also making interpretation of deposits in the volcanic record problematic.

6.3. Co-PDC plume retrieval by satellite infra-red methods

Despite the fine-grained nature of co-PDC ash, detecting dispersing co-PDC plumes using satellite ash retrieval methods remains challenging. Grain size data (Figure 6) shows that co-PDC plumes transport ash particles over great distances which are considerably coarser (median 63 – 15.6 microns) than the grain sizes accurately described by satellite retrieval methods (particles finer than 15 µm, Guéhenneux et al. 2015; Prata 1989; Stevenson et al. 2015). Furthermore, co-PDC plumes may be richer in water compared to some vent-derived ash clouds (Dartevelle et al. 2002), especially if interaction with ice, or water bodies has occurred (Scott and McGimsey 1994; Woods and Kienle 1994). As the plume rises, such water condenses and generates ice hydrometeors (Durant and Rose 2009; Durant et al. 2009; Van Eaton et al. 2012), complicating retrieval signatures, specifically in the use of 2-Band methods (e.g. Rose 2000). This results in difficulties distinguishing volcanic and meteorological clouds (Guéhenneux et al. 2015; Simpson 2000), and can lead to underestimates in plume size, as observed for the co-PDC plume associated with the November 6, 1997 dome collapse event on Montserrat (Bonadonna et al. 2002b).

7. Conclusions

Observations of co-PDC plume formation, along with the characterisation of their deposits, and insights from analogue and numerical modelling, highlight co-PDC plumes as an exceptionally efficient mechanism for transporting fine ash into the atmosphere. In intermediate size eruptions, co-PDC and vent-derived plumes are often coeval (with the exception of dome collapse events), and co-PDC deposits generally occur mixed with tephra from vent-derived plumes, producing fallout deposits with bimodal grain sizes. Comparison of grain size trends from a number of co-PDC events of varying scale show remarkable similar characteristics, despite different eruption styles and magnitudes. Specifically, ash transported in co-PDC plumes is very fine (< 90 microns) and dispersed over widespread areas without noticeable change in grain size. The small variation in grain size with distance, suggest that enhanced sedimentation associated with the formation of aggregates or gravitational instabilities dominates in co-PDC plumes, rather than individual, size-dependent, particle settling. When both form during explosive eruptions, vent-derived and co-PDC plumes can disperse synchronously within the atmosphere, complicating sedimentation behaviour.

Observations of co-PDC plume formation and results from analogue models highlight the importance of topographic control (e.g. slope changes, barriers, bends and constrictions in channels) on the formation of multiple discrete co-PDC plume pulses, and the complexities of source conditions. Multiple source regions are common, and the initial radius may be many tens of kilometres, many orders of magnitudes greater than for vent-derived plumes. Differences between vent-derived and co-PDC plume phenomena provide a cautionary note for the research community modelling and monitoring plume dispersion, and more broadly for assessing volcanic ash hazard. Co-PDC plumes need to be accounted for when assessing hazard during explosive eruptions producing PDCs, and tailored source conditions are required when numerically modelling co-PDC plume dispersion and sedimentation.

Acknowledgments

S. Engwell was funded by the People Programme (Marie Curie Actions) of the European Union's Seventh Framework Programme (FP7/2007-2013) under the project NEMOH, REA grant agreement number 289976. J. Eychenne was funded by the People Programme (Intra-European Fellowship) of the European Union's Seventh Framework Programme (FP7). We thank J. Kandlbauer, E. Gatti, A. Durant and M. Wiesner for providing raw deposit data, and K. Cashman and S. Sparks for providing reviews of an early version of the manuscript. We thank A. Rust and K. Cashman for their editorial handling of this manuscript, and E. Calder and B. Andrews for insightful and constructive reviews which greatly enhanced this manuscript.

Captions

Table 1. Examples and details of PDC-forming eruptions with associated co-PDC plume deposits for which grain size data exists in the literature. PDC Type: C – channelized deposit, B – deposit blanketing topography. Methods of grain size analysis used in each example (described in section 4.4.1): S – sieving, LD – laser diffraction, EC – electrozone counter, SR – settling rate. *Data from LaMeve database (Crosweller et al. 2012) and calculated according to Pyle (1995). ** Polymodal grain size distributions deconvolved in this study. [+]Converted volume bulk to Dense Rock Equivalent (DRE, i.e. no porosity) assuming a deposit density of 1000 kg/m^3, [++]Converted from mass to volume DRE assuming a solid density of 2500 (Mount St. Helens), 2600 (Tungurahua; Eychenne et al. 2012, and Montserrat; Bonadonna et al. 2002a) and 2200 kg/m^3 (Unzen; Watanabe et al. 1999). [1]Watanabe et al. (1999), [2]Miyabuchi (1999), [3]Bonadonna et al. (2002a), [4]Druitt et al. (2002), [5]Eychenne et al. (2013), [6]Bernard et al. (2014), [7]Eychenne et al. (2012), [8]Rose et al. (2008), [9]Davies et al. (1978), [10]Eychenne et al. 2015, [11]Sarna-Wojcicki et al. (1981), [12]Hoblitt et al. (1981), [13]Durant et al. (2009), [14]Gardner et al. (1998), [15]Beget (1983), [16]Brazier et al. (1983), [17]Carey and Sigurdsson (1986), [18]Macias et al. (1998), [19]Rose and Durant (2009), [20]Carey et al. (1995), [21]Wiesner et al. (2004), [22]Scott et al. (1996), [23] Sigurdsson et al. (1990), [24]Sparks and Huang (1980), [25]Williams (1942), [26]Williams and Goles (1968), [27]Bacon (1983), [28]Kandlbauer and Sparks (2014), [29]Sigurdsson and Carey (1989), [30]Pyle et al. (2006), [31]Fisher et al. (1993), [32]Engwell et al. (2014), [33]Rose and Chesner (1987), [34]Gatti and Oppenheimer (2012), [35]Knight and Walker (1986).

Figure 1. Comparison of the main characteristics of (**A**) vent-derived versus (**B**) co-PDC plumes. **A.** Vent-derived plumes are emitted from a point source corresponding to the top of the conduit and can be separated into three regions. The gas thrust region corresponds to the

first few hundred metres above the vent where the plume can be described as a jet due to its very high velocities, and its high density in comparison to the ambient. As the jet rises, ambient air is entrained, is heated and expands resulting in a density reduction relative to the atmosphere and the mixture rises convectively in the convective region. The final region, the umbrella, describes the height at which the plume spreads laterally into the atmosphere, and is the height at which dispersion occurs. **B.** Co-PDC plumes form as a propagating PDC sediments particles and entrains ambient air resulting in buoyancy reversal, whereby the PDC density become less than that of the ambient. The buoyant mixture detaches from the dense portion of the current, and entrains more air as it rises. Because initial vertical velocities are small and the mixture density is equivalent to the ambient, co-PDC plumes do not have a jet component, but are solely convective. In the same manner as vent-derived plumes, once the plume reaches neutral buoyancy, it spreads laterally.

Figure 2. Examples of co-PDC plumes. **A.** Co-PDC plume rising from a channel-confined PDC during the Plinian eruption of Pinatubo, Indonesia, on June 15, 1991 (photo by R. Hoblitt; PDC in the Sacobia river valley 20 km north of Pinatubo at 6:01 local time). **B.** Blast-related co-PDC plume during the Plinian eruption of Mount St. Helens, U.S., on May 18, 1980 (photo by R. Kolberg taken at ~ 15:54 GMT looking from the north-west; in Sparks et al. 1986). **C.** Co-PDC plume generated by a dome collapse on November 4, 1997 at Soufriere Hills, Montserrat (photo by E. Calder in Bonadonna et al. 2002a). **D.** Co-PDC plume generated by a dome collapse on April 21, 1990 at Redoubt volcano, Alaska (photo by R.J. Clucas). The red arrows indicate the main PDC propagation direction. The thick black arrows represent the direction and level of plume spreading. The thin black arrows indicate discrete uplift.

Figure 3. Grain size characteristics of the fallout deposit from the 39 ka Campanian ignimbrite-forming eruption from across the Mediterranean, showing the source location of the eruption (star), dispersal extent (dashed line, from Pyle et al. 2006), and locations of displayed grain size information. **A.** Grain size distributions of the basal vent-derived tephra layer and the upper co-PDC ash layer in a lake sediment core (photograph courtesy of Jens Mingram) 120 km from source. **B**, **C**, and **D.** Grain size changes with increasing distance from source within the unstratified Campanian ash layer observed in deep sea cores beyond 400 km from source. The red dashed line represents the size threshold beyond which particles are considered as fine ash (see Cashman and Rust chapter).

Figure 4. Dispersal of co-PDC deposits from dome collapse events at Soufriere Hills, Montserrat (**A** and **B**) and Mount Unzen, Japan (**C** and **D**), showing the controls of the geometry of the PDC deposits and the wind direction on the geometry and extent of the co-PDC deposits. **A** and **B.** Isopach maps (in mm) reproduced from Bonadonna et al. (2002a). **C** and **D.** Isomass maps (in g/m^2) reproduced from Watanabe et al. (1999). tr: trace of ash-fall.

Figure 5. Dispersal of mixed fallout deposits from the May 18, 1980 Mount St. Helens (**A**) and August 16, 2006 Tungurahua (**B**) eruptions showing the effect of the co-PDC contributions on the geometry of the mixed deposits. Isomass lines from (**A**) Sarna-Wojcicki et al. (1981) and (**B**) Eychenne et al. (2013). **A.** Note the displacement of the overall deposit to the north of the vent (blue arrow) due to the northern momentum of the co-PDC plume generated by the blast. **B.** Note the steep high in topography (about 500 m to 1 km high) located perpendicular to the PDC propagation direction which enhanced the formation of co-PDC plumes.

Figure 6. Grain size variations of co-PDC and mixed fallout deposits with distance from vent. The Median Diameter of the unimodal particle size distributions and coarse and fine grain size subpopulations of mixed fallout deposits are distinguished. See Table 1 for the list of eruptions and references.

References

Andrews, B.J. and Manga, M., 2011. Effects of topography on pyroclastic density current runout and formation of coignimbrites. Geology 39, 1099–1102. doi:10.1130/G32226.1

Andrews, B.J. and Manga, M., 2012. Experimental study of turbulence, sedimentation, and coignimbrite mass partitioning in dilute pyroclastic density currents. J. Volcanol. Geotherm. Res. 225-226, 30–44. doi:10.1016/j.jvolgeores.2012.02.011

Bacon, C.R., 1983. Eruptive History of Mount Mazama and Crater Lake Caldera, Cascade Range, U.S.A. J. Volcanol. Geotherm. Res. 18, 57 – 115.

Baines, P.G., Sparks, R.S.J., 2005. Dynamics of giant volcanic ash clouds from supervolcanic eruptions. Geophysical Research Letters 32, L24808.

Baxter, P.J., Bonadonna, C., Dupree, R., Hards, V.L., Kohn, S.C., Murphy, M.D., Nichols, A., Nicholson, R.A., Norton, G., Searl, A., Sparks, R.S.J. and Vickers, B.P., 1999. Cristobalite in Volcanic Ash of the Soufriere Hills Volcano, Montserrat, British West Indies. Science, 283(5405): 1142-1145

Beckett, F. M., Witham, C. S., Hort, M. C., Stevenson, J. A., Bonadonna, C., & Millington, S. C. (2014). The sensitivity of NAME forecasts of the transport of volcanic ash clouds to the physical characteristics assigned to the particles. Forecasting Research Technical Report No: 592, Met Office.

Beget, J.E., 1983. Glacier Peak, Washington: A potentially hazardous cascade volcano. Environ. Geol. 5, 83–92. doi:10.1007/BF02381101

Bernard, J., Kelfoun, K., Le Pennec, J.-L. and Vallejo Vargas, S., 2014. Pyroclastic flow erosion and bulking processes: comparing field-based vs. modeling results at Tungurahua volcano, Ecuador. Bulletin of Volcanology, 76(9).

Bonadonna, C., Ernst, G.G.J. and Sparks, R.S.J., 1998. Thickness variations and volume estimates of tephra fall deposits: the importance of particle Reynolds number. Journal of Volcanology and Geothermal Research, 81(3-4): 173-187.

Bonadonna, C., Mayberry, G.C., Calder, E.S., Sparks, R.S.J., Choux, C., Jackson, P., Lejeune, A.M., Loughlin, S.C., Norton, G.E., Rose, W.I., Ryan, G. and Young, S.R., 2002a. Tephra fallout in the eruption of Soufriere Hills Volcano, Montserrat. Geological Society, London, Memoirs, 21(1): 483-516.

Bonadonna, C., Macedonio, G. and Sparks, R.S.J., 2002b. Numerical modelling of tephra fallout associated with dome collapses and Vulcanian explosions: application to hazard assessment on Montserrat. Geological Society, London, Memoirs, 21(1): 517-537.

Bonadonna, C. and Phillips, J.C., 2003. Sedimentation from strong volcanic plumes. J. Geophys. Res., 108(B7): 2340.

Bonadonna, C. and Houghton, B.F., 2005. Total grain-size distribution and volume of tephra-fall deposits. Bulletin of Volcanology, 67(5): 441-456.

Bonadonna, C. 2006. Probabilistic modelling of tephra dispersion. *In:* H.M. Mader, S.G. Coles, C.B. Connor, L.J. Connor (Eds.), Statistics in Volcanology, Special Publications of IAVCEI (Geological Society, London), vol. 1, pp. 243–259

Brand, B.D., Mackaman-Lofland, C., Pollock, N.M., Bendaña, S., Dawson, B., Wichgers, P., 2014. Dynamics of pyroclastic density currents: Conditions that promote substrate erosion and self-channelization — Mount St Helens, Washington (USA). Journal of Volcanology and Geothermal Research 276, 189-214.

Branney, M.J., Kokelaar, P., 1997. Giant bed from a sustained catastrophic density current flowing over topography: Acatlán ignimbrite, Mexico. Geology 25, 115-118.

Branney, M. J., and Kokelaar, B. P. 2002. Pyroclastic density currents and the sedimentation of ignimbrites. Geological Society of London.

Brazier, S., Sparks, R.S.J., Carey, S.N., Sigurdsson, H. and Westgate, J.A., 1983. Bimodal grain size distribution and secondary thickening in air-fall ash layers. Nature, 301: 115-119.

Brown, R., Branney, M., 2004. Event-stratigraphy of a caldera-forming ignimbrite eruption on Tenerife: the 273 ka Poris Formation. Bulletin of Volcanology 66, 392-416.

Brown, R.J., Bonadonna, C. and Durant, A.J., 2012. A review of volcanic ash aggregation. Physics and Chemistry of the Earth, Parts A/B/C, 45-46: 65-78.

Bursik, M.I., Carey, S.N. and Sparks, R.S.J., 1992a. A gravity current model for the May 18, 1980 Mount St. Helens plume. Geophysical Research Letters, 19(16): 1663-1666.

Bursik, M.I., Sparks, R.S.J., Gilbert, J.S. and Carey, S.N., 1992b. Sedimentation of tephra by volcanic plumes: I. Theory and its comparison with a study of the Fogo A plinian deposit, Sao Miguel (Azores). Bulletin of Volcanology, 54(4): 329-344.

Bursik, M.I. and Woods, A.W., 1996. The dynamics and thermodynamics of large ash flows. Bull. Volcanol. 58, 175–193. doi:10.1007/s004450050134

Bursik, M., 2001. Effect of wind on the rise height of volcanic plumes. Geophysical Research Letters, 28(18): 3621-3624.

Caballero, L., Sarocchi, D., Soto, E. and Borselli, L., 2014. Rheological changes induced by clast fragmentation in debris flows. Journal of Geophysical Research: Earth Surface, 119(9): 2013JF002942.

Calder, E.S., Sparks, R.S.J., Woods, A.W., 1997. Dynamics of co-ignimbrite plumes generated from pyroclastic flows of Mount St. Helens (7 August 1980). Bull. Volcanol. 58, 432–440. doi:10.1007/s004450050151

Calder, E.S., Luckett, R., Sparks, R.S.J., Voight, B., 2002. Mechanisms of lava dome instability and generation of rockfalls and pyroclastic flows at Soufrière Hills Volcano, Montserrat. Geological Society, London, Memoirs 21, 173-190.

Carazzo, G. and Jellinek, A.M., 2012. A new view of the dynamics, stability and longevity of volcanic clouds. Earth and Planetary Science Letters, 325–326(0): 39-51.

Carazzo, G. and Jellinek, A.M., 2013. Particle sedimentation and diffusive convection in volcanic ash-clouds. Journal of Geophysical Research: Solid Earth, 118(4): 1420-1437.

Carey, S., Sigurdsson, H., 1986. The 1982 eruptions of El Chichon volcano, Mexico (2): Observations and numerical modelling of tephra-fall distribution. Bulletin of Volcanology 48, 127-141.

Carey, S. and Sparks, R.S.J., 1986. Quantitative models of the fallout and dispersal of tephra from volcanic eruption columns. Bulletin of Volcanology, 48(2): 109-125.

Carey, S. N., Sigurdsson, H. and Sparks, R. S. J. 1988. Experimental studies of particle□laden plumes. Journal of Geophysical Research: Solid Earth (1978–2012), 93(B12), 15314-15328.

Carey, S., Gardner, J. and Sigurdsson, H., 1995. The intensity and magnitude of Holocene plinian eruptions from Mount St. Helens volcano. J. Volcanol. Geotherm. Res. 66, 185–202. doi:10.1016/0377-0273(94)00059-P

Cashman and Rust chapter

Charbonnier, S.J., Gertisser, R., 2011. Deposit architecture and dynamics of the 2006 block-and-ash flows of Merapi Volcano, Java, Indonesia. Sedimentology 58, 1573-1612.

Cole, P. D., Calder, E. S., Druitt, T. H., Hoblitt, R., Robertson, R., Sparks, R. S. J., and Young, S. R. 1998. Pyroclastic flows generated by gravitational instability of the 1996–97 lava dome of Soufriere Hills Volcano, Montserrat. Geophysical Research Letters, 25(18), 3425-3428.

Cole, P.D., Calder, E.S., Sparks, R.S.J., Clarke, A.B., Druitt, T.H., Young, S.R., Herd, R.A., Harford, C.L., Norton, G.E., 2002. Deposits from dome-collapse and fountain-collapse pyroclastic flows at Soufrière Hills Volcano, Montserrat. Geological Society, London, Memoirs 21, 231-262.

Cole, P.D., Smith, P.J., Stinton, A.J., Odbert, H.M., Bernstein, M.L., Komorowski, J.C. and Stewart, R., 2014. Chapter 5 Vulcanian explosions at Soufrière Hills Volcano, Montserrat between 2008 and 2010. Geological Society, London, Memoirs, 39(1): 93-111.

Costa, A., Folch, A., Macedonio, G., Giaccio, B., Isaia, R. and Smith, V.C., 2012. Quantifying volcanic ash dispersal and impact of the Campanian Ignimbrite super-eruption 1–17.

Criswell, C.W., 1987. Chronology and pyroclastic stratigraphy of the May 18, 1980, Eruption of Mount St. Helens, Washington. Journal of Geophysical Research, 92(B10): 10237-10266.

Crosweller, H., Arora, B., Brown, S., Cottrell, E., Deligne, N., Guerrero, N., Hobbs, L., Kiyosugi, K., Loughlin, S., Lowndes, J., Nayembil, M., Siebert, L., Sparks, R., Takarada, S., Venzke, E., 2012. Global database on large magnitude explosive volcanic eruptions (LaMEVE). Journal of Applied Volcanology 1, 1-13.

Dartevelle, S., Ernst, G.G.J., Stix, J. and Bernard, A., 2002. Origin of the Mount Pinatubo climactic eruption cloud: Implications for volcanic hazards and atmospheric impacts. Geology, 30(7): 663-666.

Davies, D. K., Quearry, M. W., and Bonis, S. B. 1978. Glowing avalanches from the 1974 eruption of the volcano Fuego, Guatemala. Geological Society of America Bulletin, 89(3), 369-384.

Denlinger, R, P., 1987. A Model for Generation of Ash Clouds by Pyroclastic Flows, With Application to the 1980 Eruptions at Mount St . Helens, Washington 92, 10284 – 10298.

Di Muro, A., Rosi, M., Aguilera, E., Barbieri, R., Massa, G., Mundula, F. and Pieri, F., 2008. Transport and sedimentation dynamics of transitional explosive eruption columns: The example of the 800 BP Quilotoa plinian eruption (Ecuador). J. Volcanol. Geotherm. Res. 174, 307–324. doi:10.1016/j.jvolgeores.2008.03.002

Dobran, F. and Neri, A., 1993. Numerical Simulation of Collapsing Volcanic Columns. Journal of Geophysical Research: 98, 4231–4259.

Druitt, T.H., 1992. Emplacement of the 18 May 1980 lateral blast deposit ENE of Mount St. Helens, Washington. Bulletin of Volcanology, 54(7): 554-572.

Druitt, T.H., 1998. Pyroclastic density currents. Geol. Soc. London, Spec. Publ. 145, 145–182. doi:10.1144/GSL.SP.1996.145.01.08

Druitt, T.H., Young, S.R., Baptie, B., Bonadonna, C., Calder, E.S., Clarke, A.B., Cole, P.D., Harford, C., Herd, R.A., Luckett, R., Ryan, G., Voight, B., 2002. Episodes of cyclic Vulcanian explosive activity with fountain collapse at Soufriere Hills Volcano, Montserrat, in: Druitt, T.H., Kokelaar, P. (Eds.), The Eruption of Soufriere Hills Volcano, Montserrat, from 1995 to 1999. Geological Society, London, pp. 281-306.

Durant, A.J. and Rose, W.I., 2009. Sedimentological constraints on hydrometeor-enhanced particle deposition: 1992 Eruptions of Crater Peak, Alaska. Journal of Volcanology and Geothermal Research, 186(1-2): 40-59.

Durant, A.J., Rose, W.I., Sarna-Wojcicki, A.M., Carey, S. and Volentik, A.C.M., 2009. Hydrometeor-enhanced tephra sedimentation: Constraints from the 18 May 1980 eruption of Mount St. Helens. Journal of Geophysical Research, 114(B3).

Engwell, S.L., Sparks, R.S.J. and Carey, S., 2014. Physical characteristics of tephra layers in the deep sea realm: the Campanian Ignimbrite eruption. Geological Society, London, Special Publications.

Evans, J.R., Huntoon, J.E., Rose, W.I., Varley, N.R. and Stevenson, J.A., 2009. Particle sizes of andesitic ash fallout from vertical eruptions and co-pyroclastic flow clouds, Volcan de Colima, Mexico. Geology, 37(10): 935-938.

Eychenne, J., Pennec, J.-L., Troncoso, L., Gouhier, M. and Nedelec, J.-M., 2012. Causes and consequences of bimodal grain-size distribution of tephra fall deposited during the August 2006 Tungurahua eruption (Ecuador). Bulletin of Volcanology, 74(1): 187-205.

Eychenne, J., Le Pennec, J.-L., Ramón, P., Yepes, H., 2013. Dynamics of explosive paroxysms at open-vent andesitic systems: High-resolution mass distribution analyses of the 2006 Tungurahua fall deposit (Ecuador). Earth and Planetary Science Letters 361, 343-355.

Eychenne, J., Cashman, K.V., Rust, A.C. and Durant, A., 2015. Impact of the lateral blast on the spatial pattern and grain size characteristics of the May 18, 1980 Mount St. Helens fallout deposit. Journal of Geophysical Research. DOI: 10.1002/2015JB012116

Fisher, R. V., Orsi, G., Ort, M.H. and Heiken, G., 1993. Mobility of a large-volume pyroclastic flow — emplacement of the Campanian ignimbrite, Italy. J. Volcanol. Geotherm. Res. 56, 205–220. doi:10.1016/0377-0273(93)90017-L

Fisher, R., 1964. Maximum Size, Median Diameter, and Sorting of Tephra. Journal of Geophysical Research, 69: 341-355.

Folch, A., Costa, A., Durant, A. and Macedonio, G., 2010. A model for wet aggregation of ash particles in volcanic plumes and clouds: 2. Model application. Journal of Geophysical Research, 115(B9).

Folk, R.L. and Ward, W.C., 1957. Brazos River Bar: a study of the significance of grain size parameters. Journal of Sedimentary Petrology, 27: 3-26.

Freundt, A., and Schmincke, H. U. 1985. Lithic-enriched segregation bodies in pyroclastic flow deposits of Laacher See Volcano (East Eifel, Germany). Journal of volcanology and geothermal research, 25(3), 193-224.

Gardner, J.E., Carey, S. and Sigurdsson, H., 1998. Plinian eruptions at Glacier Peak and Newberry volcanoes, United States: Implications for volcanic hazards in the Cascade Range. Bull. Geol. Soc. Am. 110, 173–187. doi:10.1130/0016-7606(1998)110<0173:PEAGPA>2.3.CO;2

Gatti, E. and Oppenheimer, C., 2012. Utilization of distal tephra records for understanding climatic and environmental consequences of the Youngest Toba Tuff. Clim. Landscapes, Civilizations 198.

Gislason, S.R., Hassenkam, T., Nedel, S., Bovet, N., Eiriksdottir, E.S., Alfredsson, H.A., Hem, C.P., Balogh, Z.I., Dideriksen, K., Oskarsson, N., Sigfusson, B., Larsen, G. and Stipp, S.L.S., 2011. Characterization of Eyjafjallajökull volcanic ash particles and a protocol for rapid risk assessment. Proceedings of the National Academy of Sciences, 108(18): 7307-7312.

Guevara-Murua, A., Williams, C. A., Hendy, E. J., Rust, A. C., and Cashman, K. V. 2014. Observations of a stratospheric aerosol veil from a tropical volcanic eruption in December 1808: is this the Unknown~ 1809 eruption?. Climate of the Past, 10(5), 1707-1722.

Guéhenneux, Y., Gouhier, M. and Labazuy, P., 2015. Improved space borne detection of volcanic ash for real-time monitoring using 3-Band method. Journal of Volcanology and Geothermal Research, 293(0): 25-45.

Hay, R.L., 1959. Formation of the Crystal-Rich Glowing Avalanche Deposits of St. Vincent, B.W.I. The journal of Geology, 67: 540-562.

Herzog, M. and Graf, H.F., 2010. Applying the three-dimensional model ATHAM to volcanic plumes: Dynamic of large co-ignimbrite eruptions and associated injection heights for volcanic gases. Geophys. Res. Lett. 37. doi:10.1029/2010GL044986

Hoblitt, R.P., Miller, C.D. and Vallance, J.W., 1981. Origin and stratigraphy of the deposit produced by the May 18 directed blast. U.S. Geological Survey Professional Paper, 1250: 401-420.

Hoblitt, R.P., 1986. Observations of the eruption of July 22 and August 7, 1980, at Mount St. Helens, Washington, in: US Geological Survey Professional Paper 1335. pp. 1 –44.

Hoblitt, R.P., 2000. Was the 18 May 1980 lateral blast at Mt St Helens the product of two explosions? Phil. Trans. R. Soc. Lond., 358: 1639-1661.

Holasek, R.E. and Self, S., 1995. GOES weather satellite observations and measurements of the May 18, 1980, Mount St. Helens eruption. Journal of Geophysical Research, 100(B5): 8469.

Holasek, R.E., Self, S. and Woods, A.W., 1996. Satellite observations and interpretation of the 1991 Mount Pinatubo eruption plumes. Journal of Geophysical Research: Solid Earth, 101(B12): 27635-27655.

Horwell, C.J., Braña, L.P., Sparks, R.S.J., Murphy, M.D. and Hards, V.L., 2001. A geochemical investigation of fragmentation and physical fractionation in pyroclastic flows from the Soufrière Hills volcano, Montserrat. Journal of Volcanology and Geothermal Research, 109(4): 247-262.

Horwell, C. and Baxter, P., 2006. The respiratory health hazards of volcanic ash: a review for volcanic risk mitigation. Bull Volcanol, 69: 1 - 24.

Huppert, H., Turner, J.S., Carey, S.N., Sparks, R.S.J. and Hallworth, M.A., 1986. A laboratory simulation of pyroclastic flows down slopes. J. Volcanol. Geotherm. Res. 30, 179–199.

Inman, D.L., 1952. Measures for decribing the size distribution of sediments. Journal of Sedimentary Research, 22.

Johnston, E.N., Phillips, J.C., Bonadonna, C. and Watson, I.M., 2012. Reconstructing the tephra dispersal pattern from the Bronze Age eruption of Santorini using an advection-diffusion model. Bull. Volcanol. 74, 1485–1507. doi:10.1007/s00445-012-0609-x

Kandlbauer, J., Carey, S. and Sparks, R.S., 2013. The 1815 Tambora ash fall: implications for transport and deposition of distal ash on land and in the deep sea. Bulletin of Volcanology, 75(4): 1-11.

Kandlbauer, J., Sparks, R.S.J., 2014. New estimates of the 1815 Tambora eruption volume. Journal of Volcanology and Geothermal Research 286, 93-100.

Knight, M.D. and Walker, G.P.L., 1986. Stratigraphy, Paleomagnatism, and Magnetic fabric of the Toba tuffs: Constraints on the source and eruptive styles. J. Geophys. Res. 91, 355 – 10.

Koyaguchi, T. and Tokuno, M., 1993. Origin of the giant eruption cloud of Pinatubo, June 15, 1991. J. Volcanol. Geotherm. Res. 55, 85–96. doi:10.1016/0377-0273(93)90091-5

Kueppers, U., Cimarelli, C., Hess, K.-U., Taddeucci, J., Wadsworth, F. and Dingwell, D., 2014. The thermal stability of Eyjafjallajokull ash versus turbine ingestion test sands. Journal of Applied Volcanology, 3(1): 4.

Kuntz, M.A., Rowley, P.D., Macleod, N.S., Reynolds, R.L., McBroome, L.A., Kaplan, A.M. and Lidke, D.J., 1981. Petrography and particle-size distribution of pyroclastic-flow, ash-cloud, and surge deposits. US Geological Survey Prof Pap, 1250: 525-540.

Levine, A.H. and Kieffer, S.W., 1991. Hydraulics of the August 7, 1980, pyroclastic flow at Mount St. Helens, Washington. Geology. doi:10.1130/0091-7613(1991)019<1121

Lipman, P.W., 1967. Mineral and chemical variations within an ash-flow sheet from Aso caldera, Southwestern Japan. Contrib. to Mineral. Petrol. 16, 300–327. doi:10.1007/BF00371528

Macías, J.L., Espíndola, J.M., Bursik, M., Sheridan, M.F., 1998. Development of lithic-breccias in the 1982 pyroclastic flow deposits of El Chichón Volcano, Mexico. Journal of Volcanology and Geothermal Research 83, 173-196.

Manzella, I., Bonadonna, C., Phillips, J.C. and Monnard, H., 2015. The role of gravitational instabilities in deposition of volcanic ash. Geology, 43: 211-214.

Matthews, N.E., Smith, V.C., Costa, A., Durant, A.J., Pyle, D.M. and Pearce, N.J.G., 2012. Ultra-distal tephra deposits from super-eruptions: Examples from Toba, Indonesia and Taupo Volcanic Zone, New Zealand. Quat. Int. 258, 54–79. doi:10.1016/j.quaint.2011.07.010

Miyabuchi, Y., 1999. Deposits associated with the 1990–1995 eruption of Unzen volcano, Japan. Journal of Volcanology and Geothermal Research, 89(1–4): 139-158.

Moore, J.G. and Sisson, T.W., 1981. Deposits and effects of the May 18 pyroclastic surge. U.S. Geological Survey Professional Paper, 1250: 421-438.

Moore, J.G. and Rice, C.J., 1984. Chronology and character of the May 18, 1980, explosive eruptions of Mount St. Helens. National Academy of Sciences, Special volume on Explosive volcanism: 133-142.

Neri, A. and Dobran, F., 1994. Influence of eruption parameters on the thermofluid dynamics of collapsing volcanic columns. J. Geophys. Res. 99, 11833–11857. doi:10.1029/94JB00471

Ninkovich, D., Sparks, R.S.J., Ledbetter, M.T., 1978. The exceptional magnitude and intensity of the Toba eruption, Sumatra: an example of the use of deep-sea tephra layers as a geological tool. Bull Volcanol 41, 286-298.

Oppenheimer, C. 2002. Limited global change due to the largest known Quaternary eruption, Toba≈ 74kyr BP?. Quaternary Science Reviews, 21(14), 1593-1609.

Paladio-Melosantos, M.L.O., Solidum, R.U., Scott, W.E., Quiambao, R.B., Umbal, J.V., Rodolfo, K.S., Tubianosa, B.S., Delos Reyes, P.J., Alonso, R.A. and Ruelo, H.B., 1996. Tephra falls of the 1991 eruptions of Mount Pinatubo. In: C.G. Newhall and R. Punongbayan (Editors), Fire and mud: eruptions and lahars of Mount Pinatubo, Philippines. Philippine Institute of Volcanology and Seismology, Quezon City, and University of Washington Press, Seattle, pp. 513-536.

Pouget, S., Bursik, M., Webley, P., Dehn, J., and Pavolonis, M. 2013. Estimation of eruption source parameters from umbrella cloud or downwind plume growth rate. Journal of Volcanology and Geothermal Research, 258, 100-112.

Prata, A. J. 1989. Observations of volcanic ash clouds in the 10-12 μm window using AVHRR/2 data. International Journal of Remote Sensing, 10(4-5), 751-761.

Pyle, D.M., 1995. Mass and energy budgets of explosive volcanic eruption. Geophys Res Lett 22, 563-566.

Pyle, D.M., Ricketts, G.D., Margari, V., van Andel, T.H., Sinitsyn, A. A., Praslov, N.D. and Lisitsyn, S., 2006. Wide dispersal and deposition of distal tephra during the Pleistocene "Campanian Ignimbrite/Y5" eruption, Italy. Quat. Sci. Rev. 25, 2713–2728. doi:10.1016/j.quascirev.2006.06.008

Ritchie, L.J., Cole, P.D., Sparks, R.S.J., 2002. Sedimentology of deposits from the pyroclastic density current of 26 December 1997 at Soufrière Hills Volcano, Montserrat. Geological Society, London, Memoirs 21, 435-456.

Rose, W.I. and Chesner, C. A., 1987. Dispersal of ash in the great Toba eruption, 75 ka. Geology 15, 913–917. doi:10.1130/0091-7613(1987)15<913:DOAITG>2.0.CO;2

Rose, W.I., Bluth, G.J.S. and Ernst, G.G.J., 2000. Integrating retrievals of volcanic cloud characteristics from satellite remote sensors: a summary. Philos. Trans. R. Soc. A Math. Phys. Eng. Sci. 358, 1585–1606. doi:10.1098/rsta.2000.0605

Rose, W., Self, S., Murrow, P., Bonadonna, C., Durant, A. and Ernst, G., 2008. Nature and significance of small volume fall deposits at composite volcanoes: Insights from the October 14, 1974 Fuego eruption, Guatemala. Bulletin of Volcanology, 70(9): 1043-1067.

Rose, W. and Durant, A., 2009. Fine ash content of explosive eruptions. J Volcanol Geotherm Res, 186: 32 - 39.

Rose, W.I. and Durant, A.J., 2011. Fate of volcanic ash: Aggregation and fallout. Geology, 39(9): 895-896.

Rosi, M., Vezzoli, L., Castelmenzano, A. and Grieco, G., 1999. Plinian pumice fall deposit of the Campanian Ignimbrite eruption (Phlegraean Fields, Italy). J. Volcanol. Geotherm. Res. 91, 179–198.

Rosi, M., Paladio-Melosantos, M., Di Muro, A., Leoni, R. and Bacolcol, T., 2001. Fall vs flow activity during the 1991 climactic eruption of Pinatubo Volcano (Philippines). Bulletin of Volcanology, 62(8): 549-566.

Rosi, M., Bertagnini, A., Harris, A., Pioli, L., Pistolesi, M., Ripepe, M., 2006. A case history of paroxysmal explosion at Stromboli: Timing and dynamics of the April 5, 2003 event. Earth and Planetary Science Letters 243, 594-606.

Sarna-Wojcicki, A., Shipley, S., Waitt, R.B., Dzurisin, D. and Wood, S., 1981. Aeral distribution, thickness , mass, volume and grain size of air-fall ash from the six major eruptions of 1980. U.S. Geological Survey Professional Paper, 1250: 577-600.

Scarpati, C., Sparice, D. and Perrotta, A., 2014. A crystal concentration method for calculating ignimbrite volume from distal ash-fall deposits and a reappraisal of the magnitude of the Campanian Ignimbrite. J. Volcanol. Geotherm. Res. 280, 67–75. doi:10.1016/j.jvolgeores.2014.05.009

Scott, W.E., McGimsey, R.G., 1994. Character, mass, distribution, and origin of tephra-fall deposits of the 1989-1990 eruption of Redoubt Volcano, south-central Alaska. Journal of Volcanology and Geothermal Research 62, 251-272.

Scott, W.E., Hoblitt, R.P., Torres, R.C., Self, S., Martinez, M.L. and Nillos, T., 1996. Pyroclastic flows of the June 15, 1991, climactic eruption of Mount Pinatubo. In: C.G. Newhall and R. Punongbayan (Editors), Fire and Mud: Eruptions and Lahars of Mount Pinatubo, Philippines. Philippine Institute of Volcanology and Seismology, Quezon City, and University of Washington Press, Seattle.

Sigurdsson, H. and Carey, S., 1989. Plinian and co-ignimbrite tephra fall from the 1815 eruption of Tambora volcano. Bulletin of Volcanology, 51(4): 243-270.

Sigurdsson, H., Carey, S., & Devine, J. D., 1990. Assessment of mass, dynamics and environmental effects of the Minoan eruption of Santorini volcano. Thera and the Aegean world III, *2*, 100-112.

Simpson, J., 2000. Failures in Detecting Volcanic Ash from a Satellite-Based Technique. Remote Sens. Environ. 72, 191–217. doi:10.1016/S0034-4257(99)00103-0

Sparks, R.S.J., Self, S. and Walker, G.P.L., 1973. Products of Ignimbrite Eruptions. Geology, 1(3): 115-118.

Sparks, R.S.J., 1975. Stratigraphy and geology of the ignimbrites of Vulsini volcano, Central Italy. *Geologische Rundschau*, *64*(1), 497-523.

Sparks, R.S.J., 1976. Grain size variations in ignimbrites and implications for the transport of pyroclastic flows. Sedimentology 23, 147–188. doi:10.1111/j.1365-3091.1976.tb00045.x

Sparks, R.S.J. and Wilson, L., 1976. A model for the formation of ignimbrite by gravitational column collapse. J. Geol. Soc. London 132, 441–451. doi:10.1144/gsjgs.132.4.0441

Sparks, R.S.J. and Walker, G.P.L., 1977. The significance of vitric-enriched air-fall ashes associated with crystal-enriched ignimbrites. Journal of Volcanology and Geothermal Research, 2: 329-341.

Sparks, R.S.J. 1978. Gas release rates from pyroclastic flows: a assessment of the role of fluidisation in their emplacement. *Bulletin Volcanologique*, *41*(1), 1-9.

Sparks, R.S.J. and Huang, T.C., 1980. The volcanological significance of deep-sea ash layers associated with ignimbrites. Geological Magazine, 117: 425-436.

Sparks, R.S.J., Brazier, S., Huang, T.C. and Muerdter, D., 1984. Sedimentology of the Minoan deep-sea tephra layer in the Aegean and eastern Mediterranean. Marine Geology, 54: 131-167.

Sparks, R.S.J., 1986. The dimensions and dynamics of volcanic eruption columns. Bulletin of Volcanology, 48(1): 3-15.

Sparks, R.S.J., Moore, J.G. and Rice, C.J., 1986. The initial giant umbrella cloud of the May 18th, 1980, explosive eruption of Mount St. Helens. Journal of Volcanology and Geothermal Research, 28: 257-274.

Sparks, R.S.J., Bursik, M.I., Ablay, G.J., Thomas, R.M.E. and Carey, S.N., 1992. Sedimentation of tephra by volcanic plumes. Part 2: controls on thickness and grain-size variations of tephra fall deposits. Bulletin of Volcanology, 54(8): 685-695.

Sparks, R. S. J., Bonnecaze, R. T., Huppert, H. E., Lister, J. R., Hallworth, M. A., Mader, H., and Phillips, J. 1993. Sediment-laden gravity currents with reversing buoyancy. Earth and Planetary Science Letters, 114(2), 243-257.

Sparks, R.S.J., Bursik, M.I., Carey, S.N., Gilbert, J., Glaze, L.S., Sigurdsson, H. and Woods, A.W., 1997. Volcanic Plumes. Wiley.

Stevenson, J. A., Millington, S. C., Beckett, F. M., Swindles, G. T. and Thordarson, T. 2015. Big grains go far: reconciling tephrochronology with atmospheric measurements of volcanic ash. Atmospheric Measurement Techniques Discussions, 8(1), 65-120.

Stinton, A.J., Cole, P.D., Stewart, R.C., Odbert, H.M. and Smith, P., 2014. Chapter 7 The 11 February 2010 partial dome collapse at Soufrière Hills Volcano, Montserrat. Geological Society, London, Memoirs, 39(1): 133-152.

Taddeucci, J., Scarlato, P., Montanaro, C., Cimarelli, C., Del Bello, E., Freda, C., Andronico, D., Gudmundsson, M.T. and Dingwell, D.B., 2011. Aggregation-dominated ash settling from the Eyjafjallajokull volcanic cloud illuminated by field and laboratory high-speed imaging. Geology, 39(9): 891-894.

Van Eaton, A., Muirhead, J., Wilson, C.N. and Cimarelli, C., 2012. Growth of volcanic ash aggregates in the presence of liquid water and ice: an experimental approach. Bulletin of Volcanology, 74(9): 1963-1984.

Van Eaton, A.R. and Wilson, C.J.N., 2013. The nature, origins and distribution of ash aggregates in a large-scale wet eruption deposit: Oruanui, New Zealand. Journal of Volcanology and Geothermal Research, 250(0): 129-154.

Walker, G.P.L., 1972. Crystal concentration in ignimbrites. Contrib Mineral Petrol, 36: 135-146.

Watanabe, K., Ono, K., Sakaguchi, K., Takada, A. and Hoshizumi, H., 1999. Co-ignimbrite ash-fall deposits of the 1991 eruptions of Fugen-dake, Unzen Volcano, Japan. Journal of Volcanology and Geothermal Research, 89(1–4): 95-112.

Wiesner, M.G., Wang, Y., Zheng, L., 1995. Fallout of volcanic ash to the deep South China Sea induced by the 1991 eruption of Mount Pinatubo (Philippines). Geology 23, 885.

Wiesner, M.G., Wetzel, A., Catane, S.G., Listanco, E.L. and Mirabueno, H.T., 2004. Grain size, areal thickness distribution and controls on sedimentation of the 1991 Mount Pinatubo tephra layer in the South China Sea. Bulletin of Volcanology, 66(3): 226-242.

Williams, H. The Geology of Crater Lake National Park, Oregon: With a Reconnaissance of the Cascade Range Southward to Mount Shasta. Vol. 540. Carnegie institution, 1942.

Williams, H. and Goles, G., 1968. Volume of the Mazama Ash-fall and the origin of Crater Lake Caldera, in: Andesite Conference Guidebook. pp. 37 – 41.

Wilson, L., Sparks, R. S. J., and Walker, G. P. 1980. Explosive volcanic eruptions—IV. The control of magma properties and conduit geometry on eruption column behaviour. Geophysical Journal International, 63(1), 117-148.

Wohletz, K.H., Sheridan, M.F. and Brown, W.K., 1989. Particle Size Distributions and the Sequential Fragmentation/Transport Theory Applied to Volcanic Ash. J. Geophys. Res., 94(B11): 15703-15721.

Woods, A.W. and Wohletz, K.H., 1991. Dimensions and dynamics of co-ignimbrite eruption columns. Nature 350, 225–227.

Woods, A. W., and Caulfield, C. C. P. 1992. A laboratory study of explosive volcanic eruptions. Journal of Geophysical Research: Solid Earth (1978–2012), 97(B5), 6699-6712.

Woods, A.W. and Kienle, J., 1994. The dynamics and thermodynamics of volcanic clouds: Theory and observations from the april 15 and april 21, 1990 eruptions of redoubt volcano, Alaska. Journal of Volcanology and Geothermal Research, 62(1–4): 273-299.

Woods, A. W., and Bursik, M. I. 1994. A laboratory study of ash flows. Journal of Geophysical Research: Solid Earth (1978–2012), 99(B3), 4375-4394.

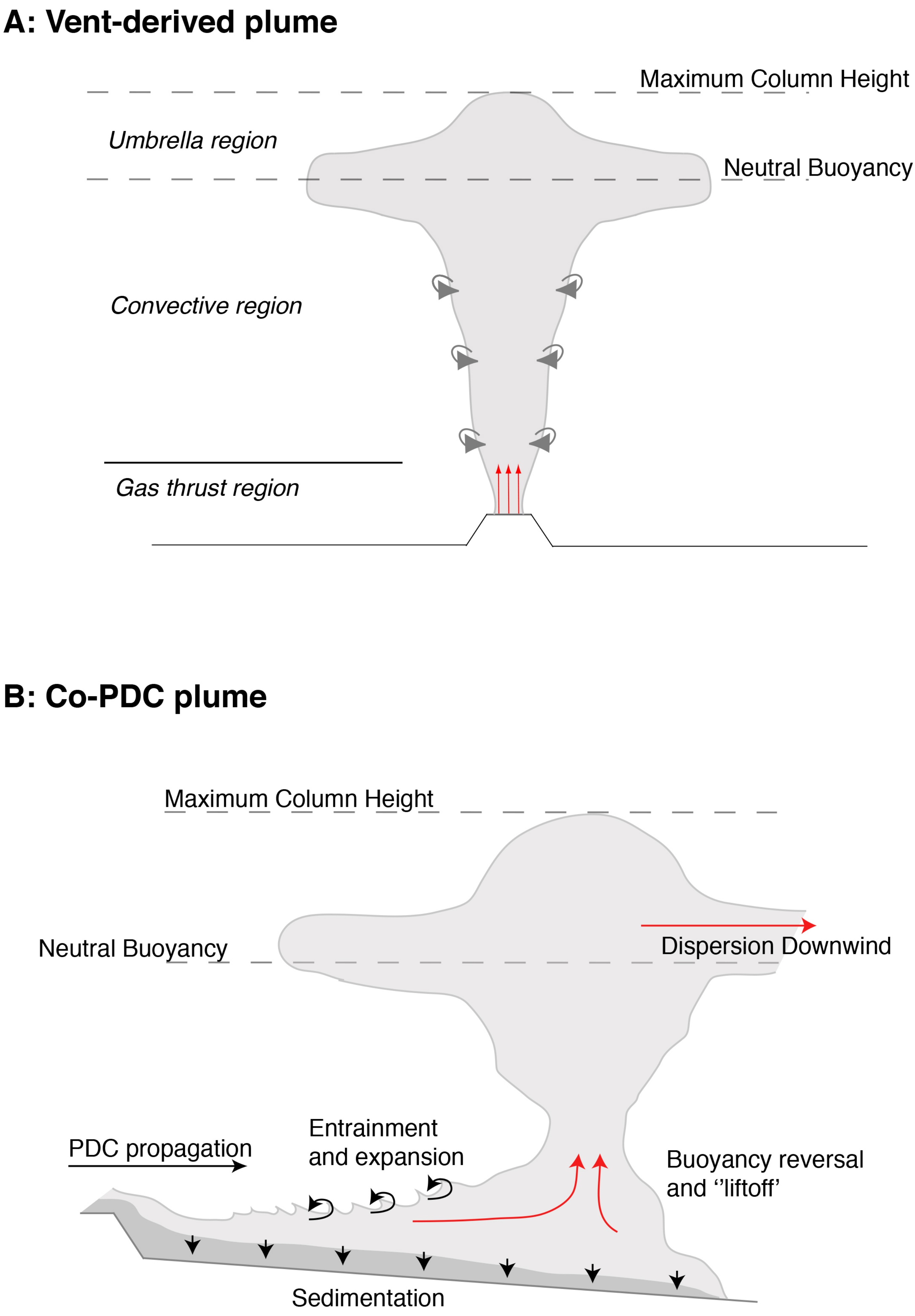

A: Vent-derived plume
Maximum Column Height
Umbrella region
Neutral Buoyancy
Convective region
Gas thrust region
B: Co-PDC plume
Maximum Column Height
Neutral Buoyancy
Dispersion Downwind
Entrainment
and expansion
PDC propagation
Buoyancy reversal
and ''liftoff'
Sedimentation

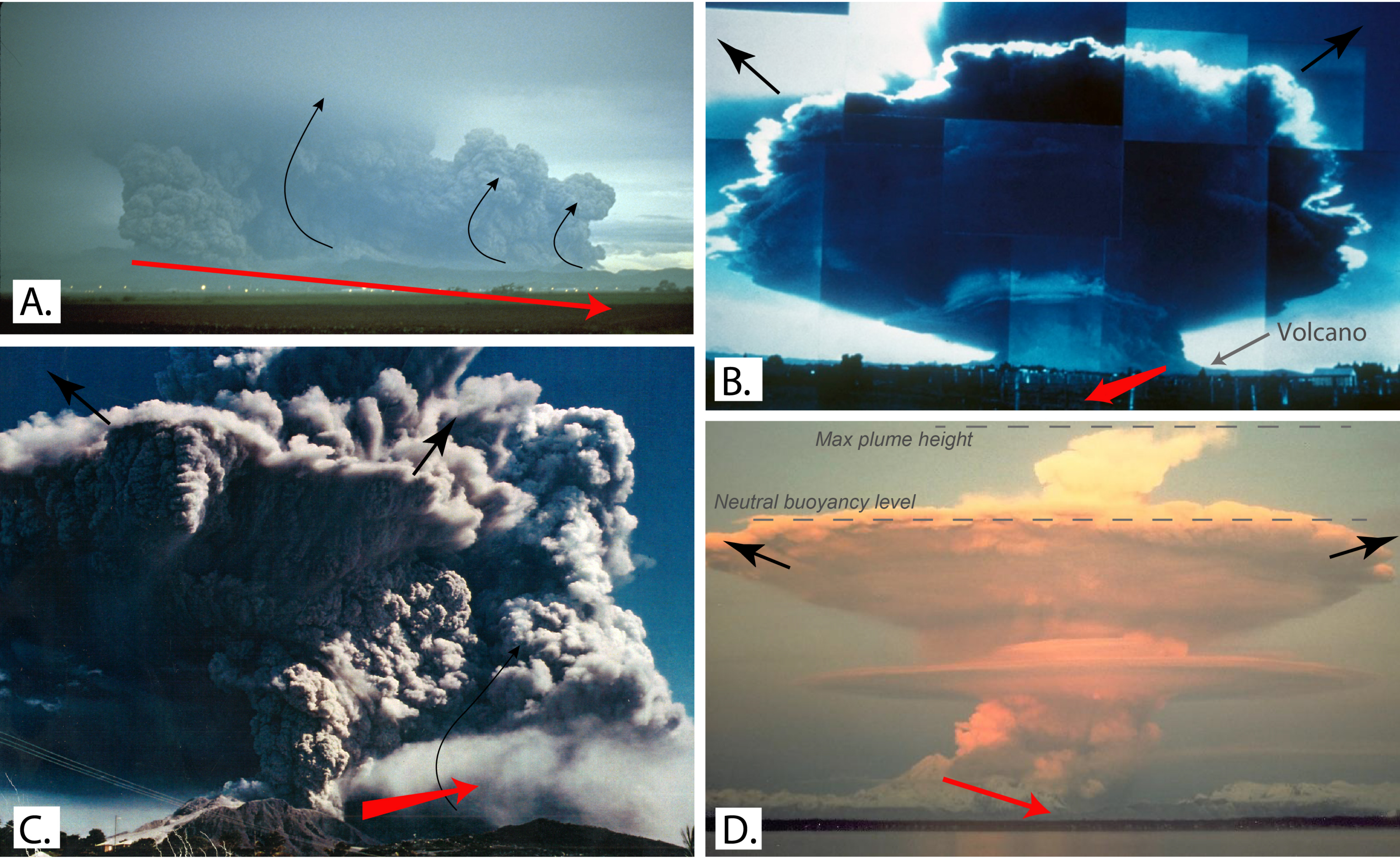
A.
B.
Volcano
C.
D.
Max plume height
Neutral buoyancy level

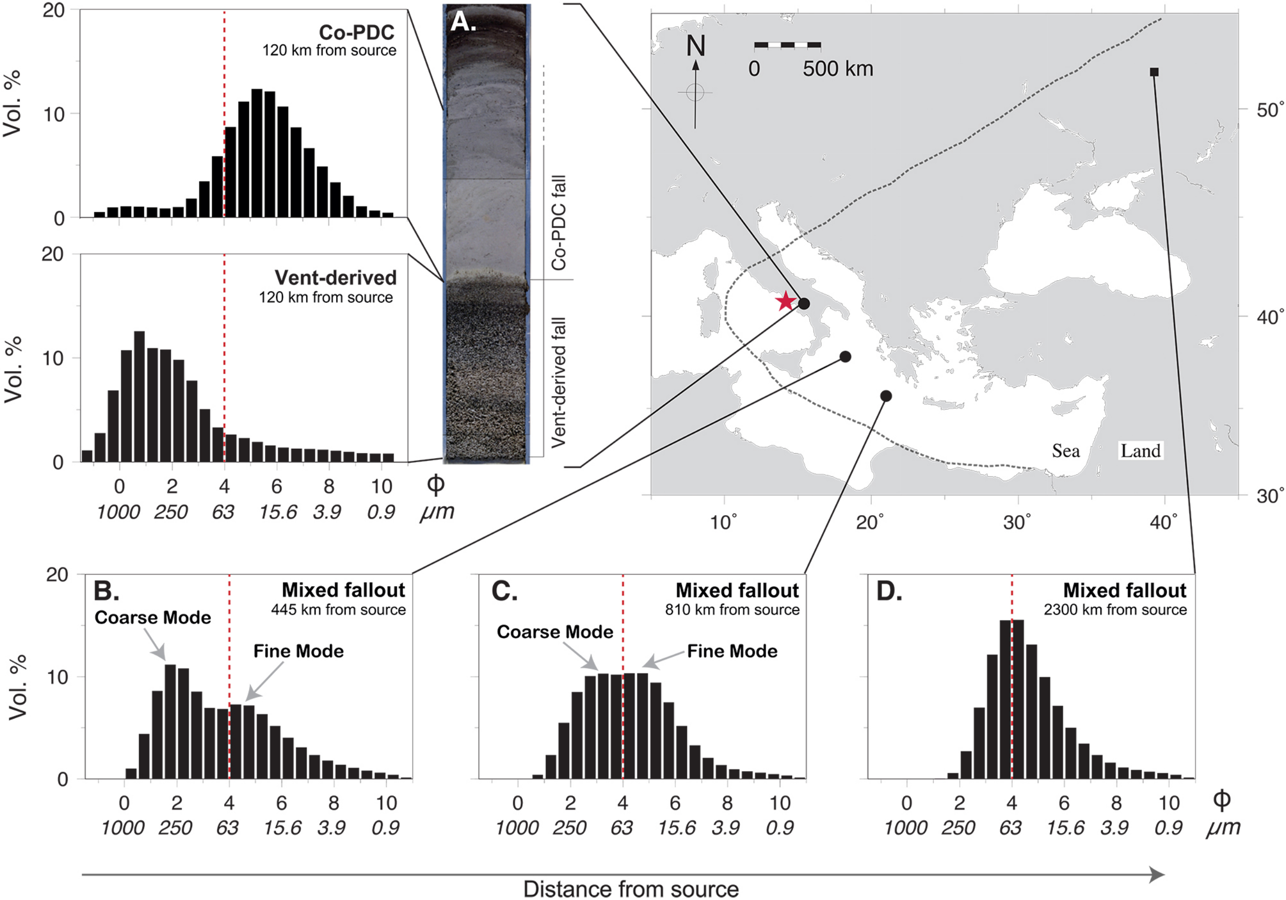

A.
Co-PDC
120 km from source
Vent-derived
120 km from source
Co-PDC fall
Vent-derived fall
Vol. %
0
10
20
Φ
μm
0 2 4 6 8 10
1000 250 63 15.6 3.9 0.9
N
0 500 km
50˚
40˚
30˚
10˚ 20˚ 30˚ 40˚
Sea
Land
B.
Mixed fallout
445 km from source
Coarse Mode
Fine Mode
C.
Mixed fallout
810 km from source
Coarse Mode
Fine Mode
D.
Mixed fallout
2300 km from source
Distance from source

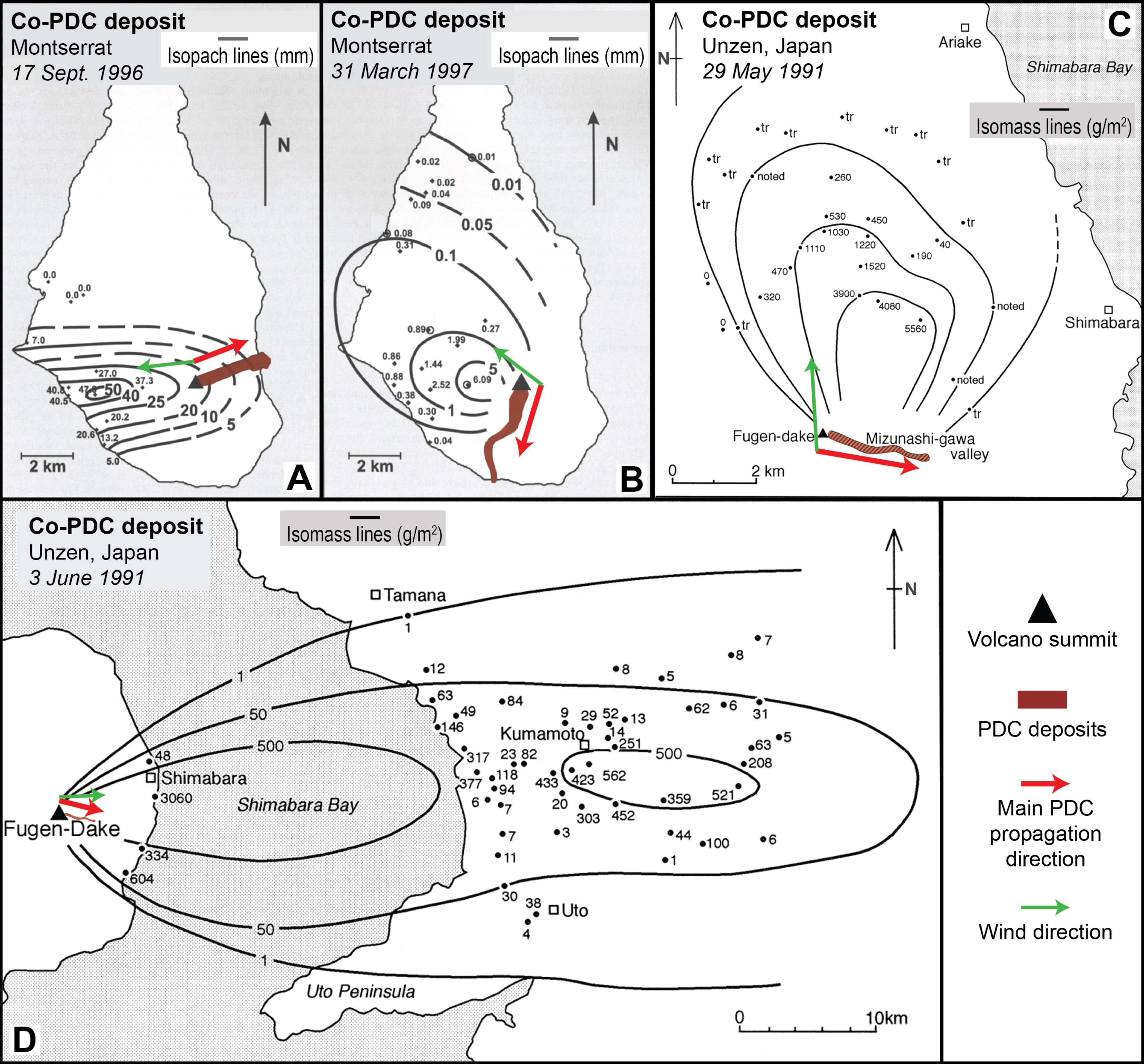

Co-PDC deposit
Montserrat
17 Sept. 1996
Isopach lines (mm)
N
2 km
A
Co-PDC deposit
Montserrat
31 March 1997
Isopach lines (mm)
N
2 km
B
Co-PDC deposit
Unzen, Japan
29 May 1991
Isomass lines (g/m2)
Ariake
Shimabara Bay
Shimabara
Fugen-dake
Mizunashi-gawa valley
0 2 km
C
Co-PDC deposit
Unzen, Japan
3 June 1991
Isomass lines (g/m2)
Tamana
Kumamoto
Shimabara
Shimabara Bay
Fugen-Dake
Uto
Uto Peninsula
0 10km
D
Volcano summit
PDC deposits
Main PDC propagation direction
Wind direction

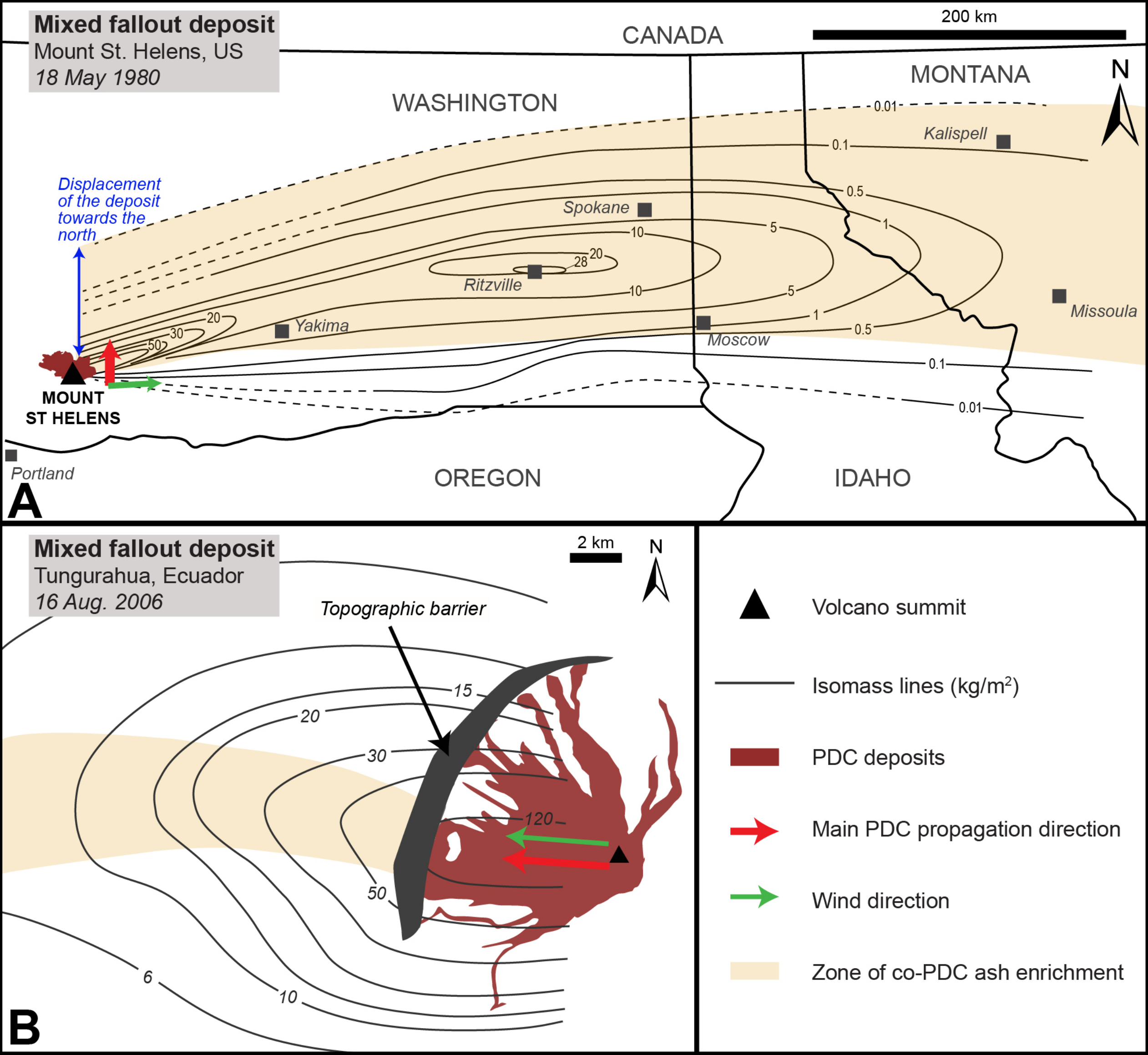

Mixed fallout deposit
Mount St. Helens, US
18 May 1980
200 km
CANADA
WASHINGTON
MONTANA
N
0.01
0.1
0.5
1
5
10
20
28
30
50
Kalispell
Spokane
Ritzville
Yakima
Moscow
Missoula
Portland
Displacement of the deposit towards the north
MOUNT ST HELENS
OREGON
IDAHO
A
Mixed fallout deposit
Tungurahua, Ecuador
16 Aug. 2006
2 km
N
Topographic barrier
6
10
15
20
30
50
120
B
Volcano summit
Isomass lines (kg/m²)
PDC deposits
Main PDC propagation direction
Wind direction
Zone of co-PDC ash enrichment

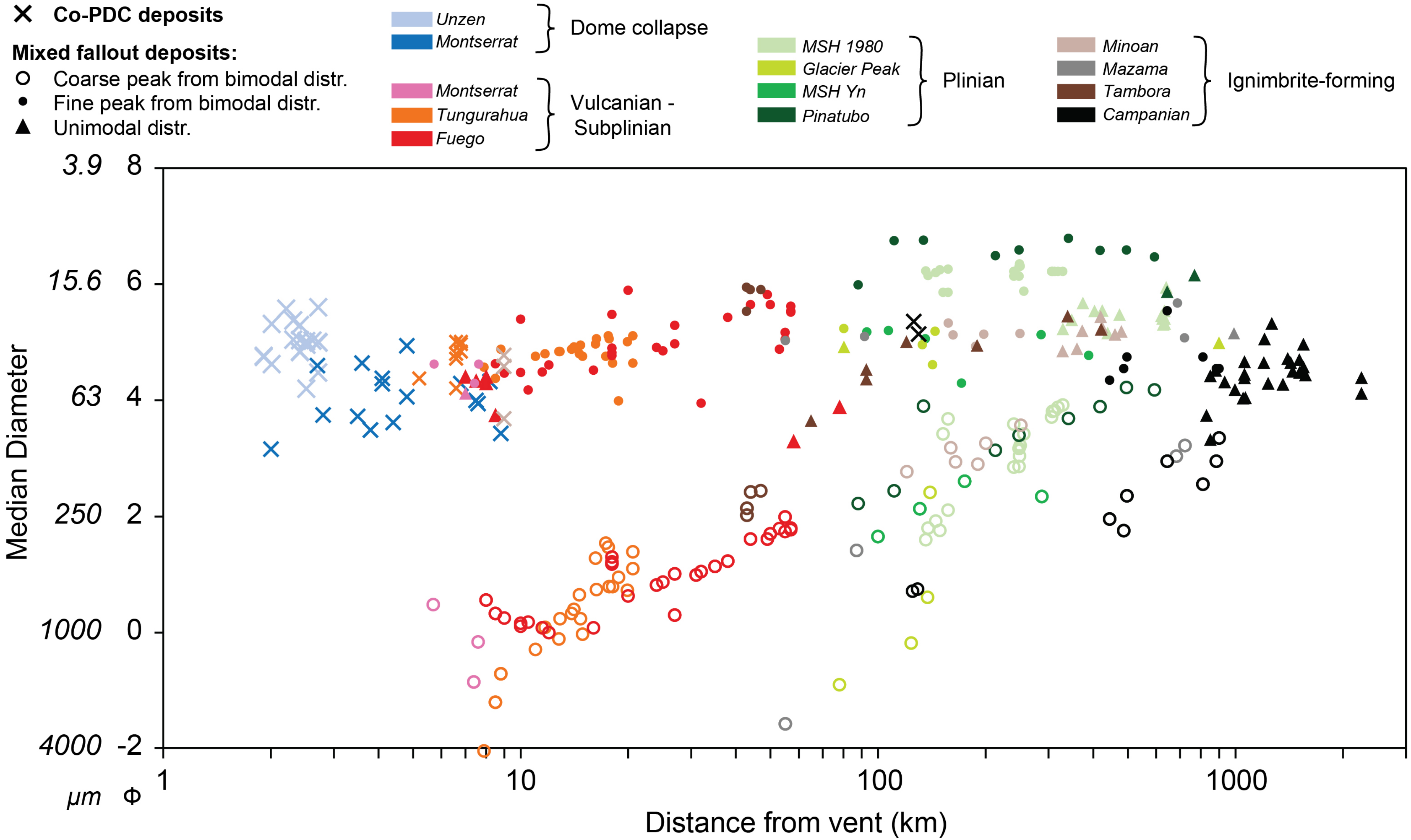
Co-PDC deposits
Mixed fallout deposits:
Coarse peak from bimodal distr.
Fine peak from bimodal distr.
Unimodal distr.
Unzen
Montserrat
Dome collapse
Montserrat
Tungurahua
Fuego
Vulcanian - Subplinian
MSH 1980
Glacier Peak
MSH Yn
Pinatubo
Plinian
Minoan
Mazama
Tambora
Campanian
Ignimbrite-forming
Median Diameter
μm
Φ
3.9
8
15.6
6
63
4
250
2
1000
0
4000
-2
1
10
100
1000
Distance from vent (km)

Table 1. Examples and details of PDC-forming eruptions with associated co-PDC plume deposits for which grain size data exists in the literature. PDC Type: C – channelized deposit, B – deposit blanketing topography. Methods of grain size analysis used in each example (described in section 4.4.1): S – sieving, LD – laser diffraction, EC – electrozone counter, SR – settling rate. *Data from LaMeve database (Crosweller et al. 2012) and calculated according to Pyle (1995). ** Polymodal grain size distributions deconvolved in this study. $^{+}$Converted volume bulk to Dense Rock Equivalent (DRE, i.e. no porosity) assuming a deposit density of 1000 kg/m^3, $^{++}$Converted from mass to volume DRE assuming a solid density of 2500 (Mount St. Helens), 2600 (Tungurahua; Eychenne et al. 2012, and Montserrat; Bonadonna et al. 2002a) and 2200 kg/m^3 (Unzen; Watanabe et al. 1999). (1)Watanabe et al. (1999), (2)Miyabuchi (1999), (3)Bonadonna et al. (2002a), (4)Druitt et al. (2002), (5)Eychenne et al. (2013), (6)Bernard et al. (2014), (7)Eychenne et al. (2012), (8)Rose et al. (2008), (9)Davies et al. (1978), (10)Eychenne et al. 2015, (11)Sarna-Wojcicki et al. (1981), (12)Hoblitt et al. (1981), (13)Durant et al. (2009), (14)Gardner et al. (1998), (15)Beget (1983), (16)Brazier et al. (1983), (17)Carey and Sigurdsson (1986), (18)Macias et al. (1998), (19)Rose and Durant (2009), (20)Carey et al. (1995), (21)Wiesner et al. (2004), (22)Scott et al. (1996), (23) Sigurdsson et al. (1990), (24)Sparks and Huang (1980), (25)Williams (1942), (26)Williams and Goles (1968), (27)Bacon (1983), (28)Kandlbauer and Sparks (2014), (29)Sigurdsson and Carey (1989), (30)Pyle et al. (2006), (31)Fisher et al. (1993), (32)Engwell et al. (2014), (33)Rose and Chesner (1987), (34)Gatti and Oppenheimer (2012), (35)Knight and Walker (1986).

A: Vent-derived plume

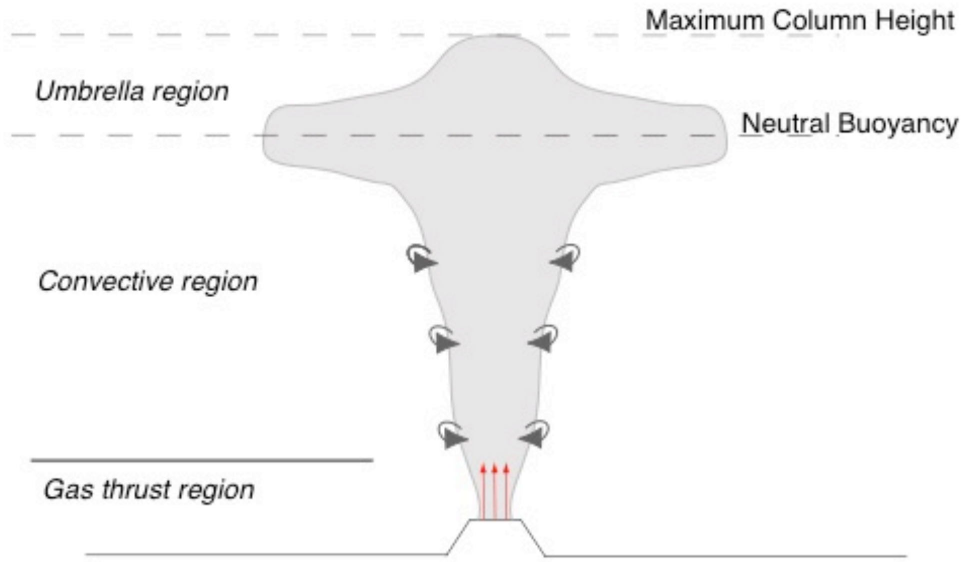

B: Co-PDC plume

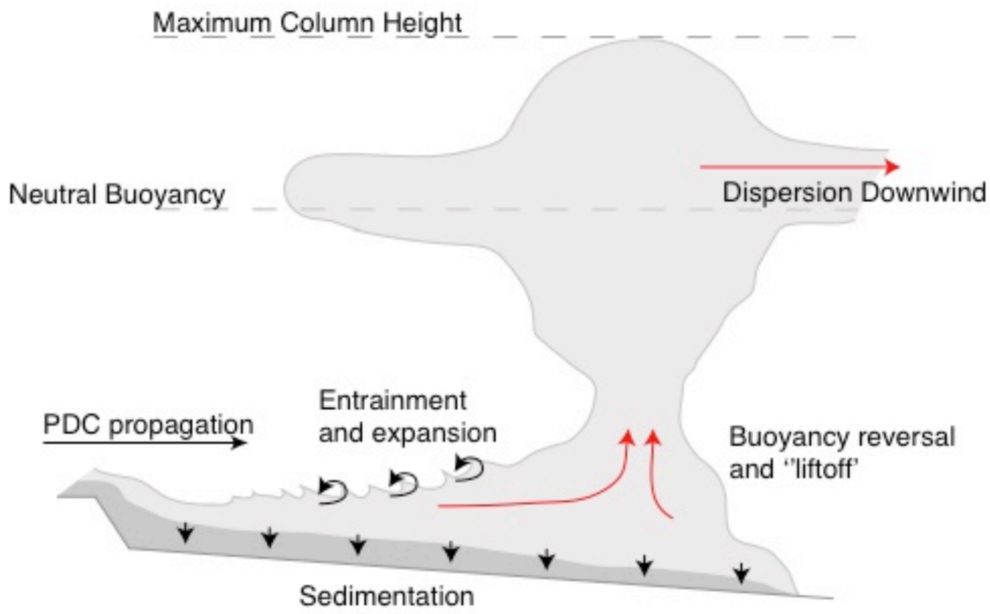

Figure 1. Comparison of the main characteristics of vent-derived **(A)** versus co-PDC plumes **(B)**. **A.** Vent-derived plumes are emitted from a point source corresponding to the top of the conduit and can be separated into three regions. The gas thrust region corresponds to the first few hundred metres above the vent where the plume can be described as a jet due to its very high velocities, and its high density in comparison to the ambient. As the jet rises, ambient air is entrained, is heated and expands resulting in a density reduction relative to the atmosphere and the mixture rises convectively in the convective region. The final region, the umbrella, describes the height at which the plume spreads laterally into the atmosphere, and is the height at which dispersion occurs. **B.** Co-PDC plumes form as a propagating PDC sediments particles and entrains ambient air resulting in buoyancy reversal, whereby the PDC density become less than that of the ambient. The buoyant mixture detaches from the dense portion of the current, and entrains more air as it rises. Because initial vertical velocities are small and the mixture density is equivalent to the ambient, co-PDC plumes do not have a jet component, but are solely convective. In the same manner as vent-derived plumes, once the plume reaches neutral buoyancy, it spreads laterally.

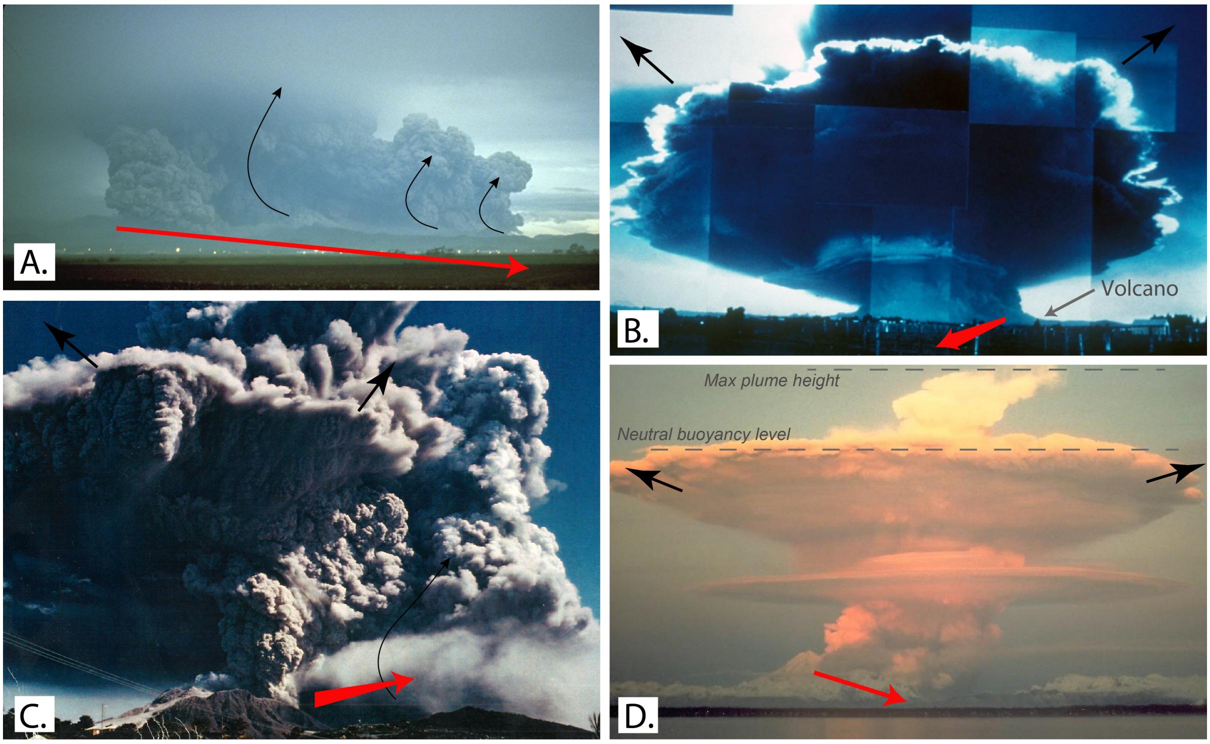

Figure 2. Examples of co-PDC plumes. **A.** Co-PDC plume rising from a channel-confined PDC during the Plinian eruption of Pinatubo, Indonesia, on June 15, 1991 (photo by R. Hoblitt; PDC in the Sacobia river valley 20 km north of Pinatubo at 6:01 local time). **B.** Blast-related co-PDC plume during the Plinian eruption of Mount St. Helens, U.S., on May 18, 1980 (photo by R. Kolberg taken at ~ 15:54 GMT looking from the north-west; in Sparks et al. 1986). **C.** Co-PDC plume generated by a dome collapse on November 4, 1997 at Soufriere Hills, Montserrat (photo by E. Calder in Bonadonna et al. 2002a). **D.** Co-PDC plume generated by a dome collapse on April 21, 1990 at Redoubt volcano, Alaska (photo by R.J. Clucas). The red arrows indicate the main PDC propagation direction. The thick black arrows represent the direction and level of plume spreading. The thin black arrows indicate discrete uplift.

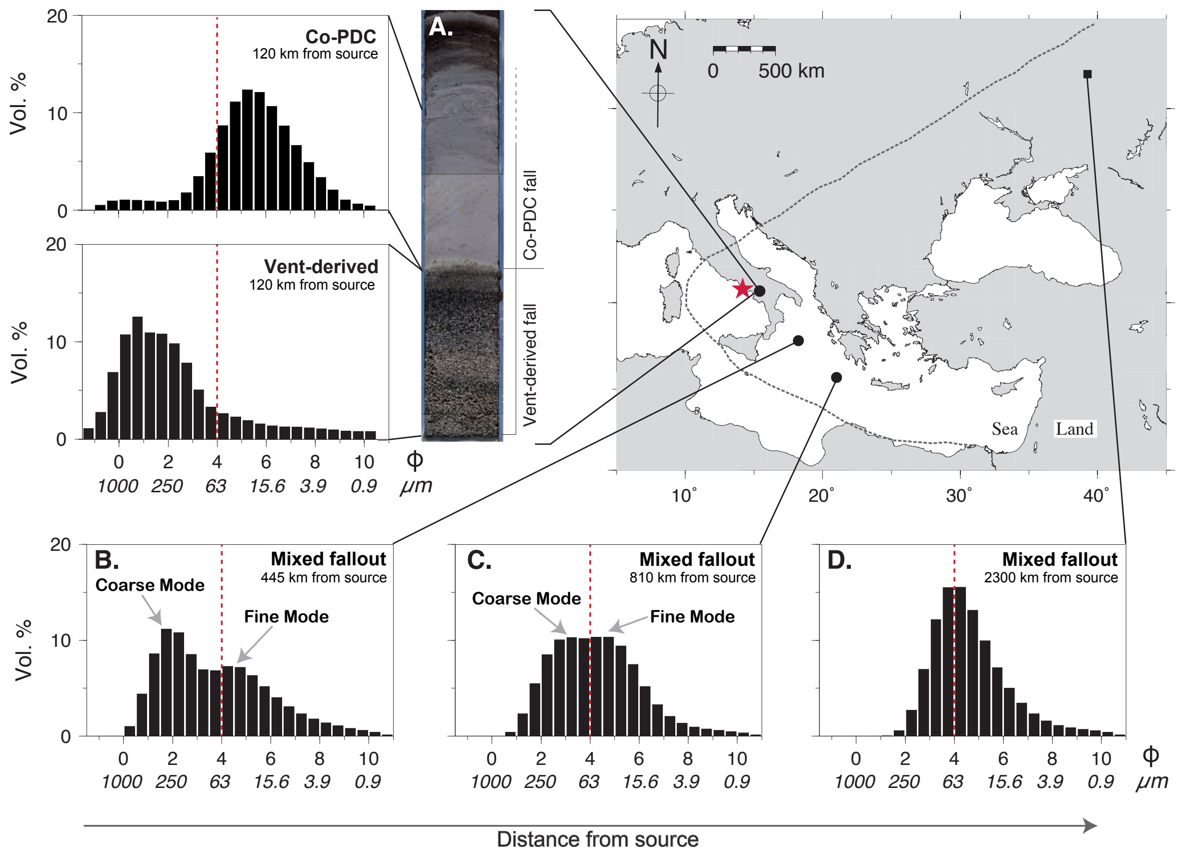

Figure 3. Grain size characteristics of the fallout deposit from the 39 ka Campanian ignimbrite-forming eruption from across the Mediterranean, showing the source location of the eruption (star), dispersal extent (dashed line, from Pyle et al. 2006), and locations of displayed grain size information. **A.** Grain size distributions of the basal vent-derived tephra layer and the upper co-PDC ash layer in a lake sediment core (photograph courtesy of Jens Mingram) 120 km from source. **B**, **C**, and **D.** Grain size changes with increasing distance from source within the unstratified Campanian ash layer observed in deep sea cores beyond 400 km from source. The red dashed line represents the size threshold beyond which particles are considered as fine ash (see Cashman and Rust chapter).

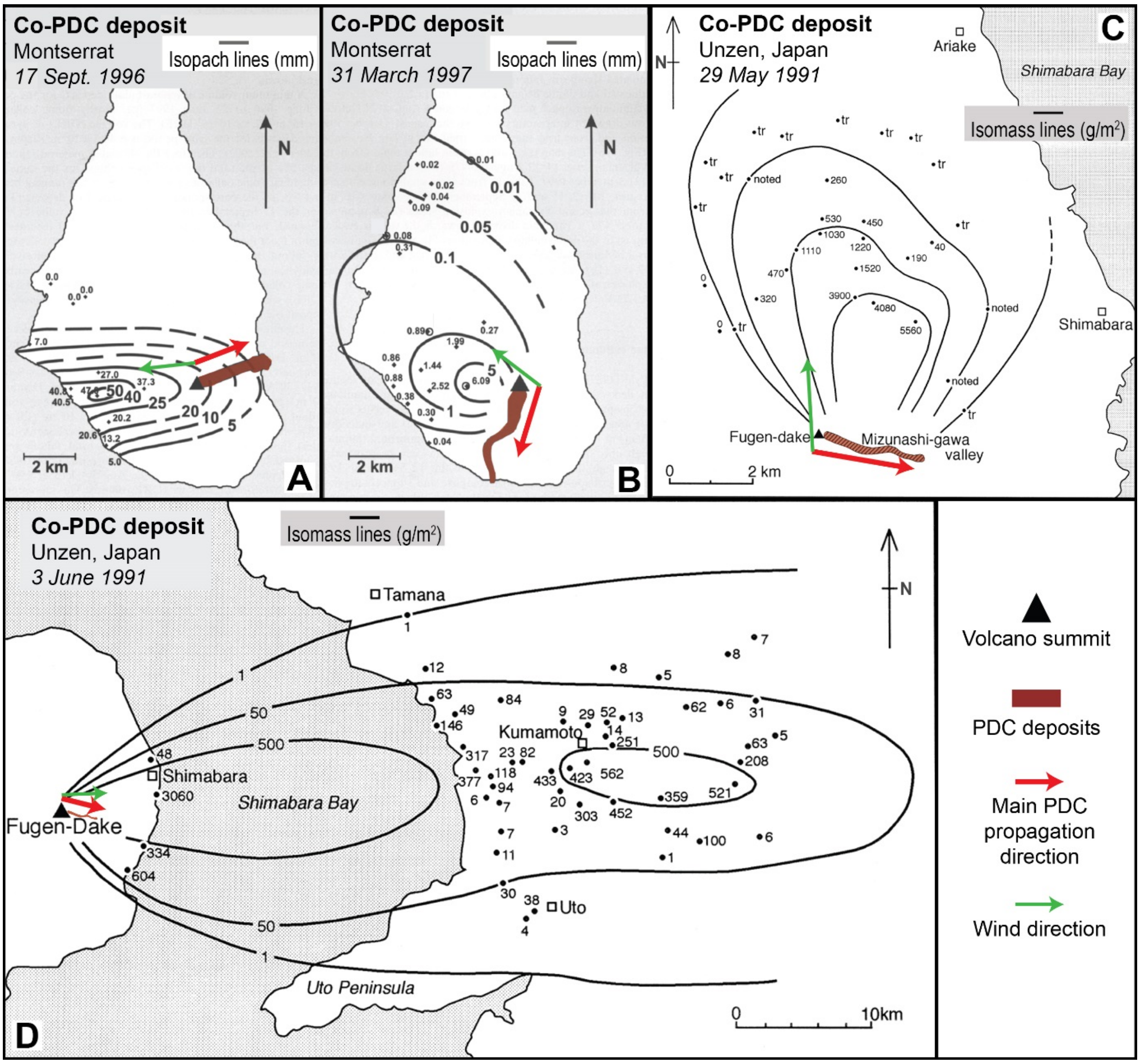

Figure 4. Dispersal of co-PDC deposits from dome collapse events at Soufriere Hills, Montserrat (**A** and **B**) and Mount Unzen, Japan (**C** and **D**), showing the controls of the geometry of the PDC deposits and the wind direction on the geometry and extent of the co-PDC deposits. **A** and **B.** Isopach maps (in mm) reproduced from Bonadonna et al. (2002a). **C** and **D.** Isomass maps (in g/m^2) reproduced from Watanabe et al. (1999). tr: trace of ash-fall.

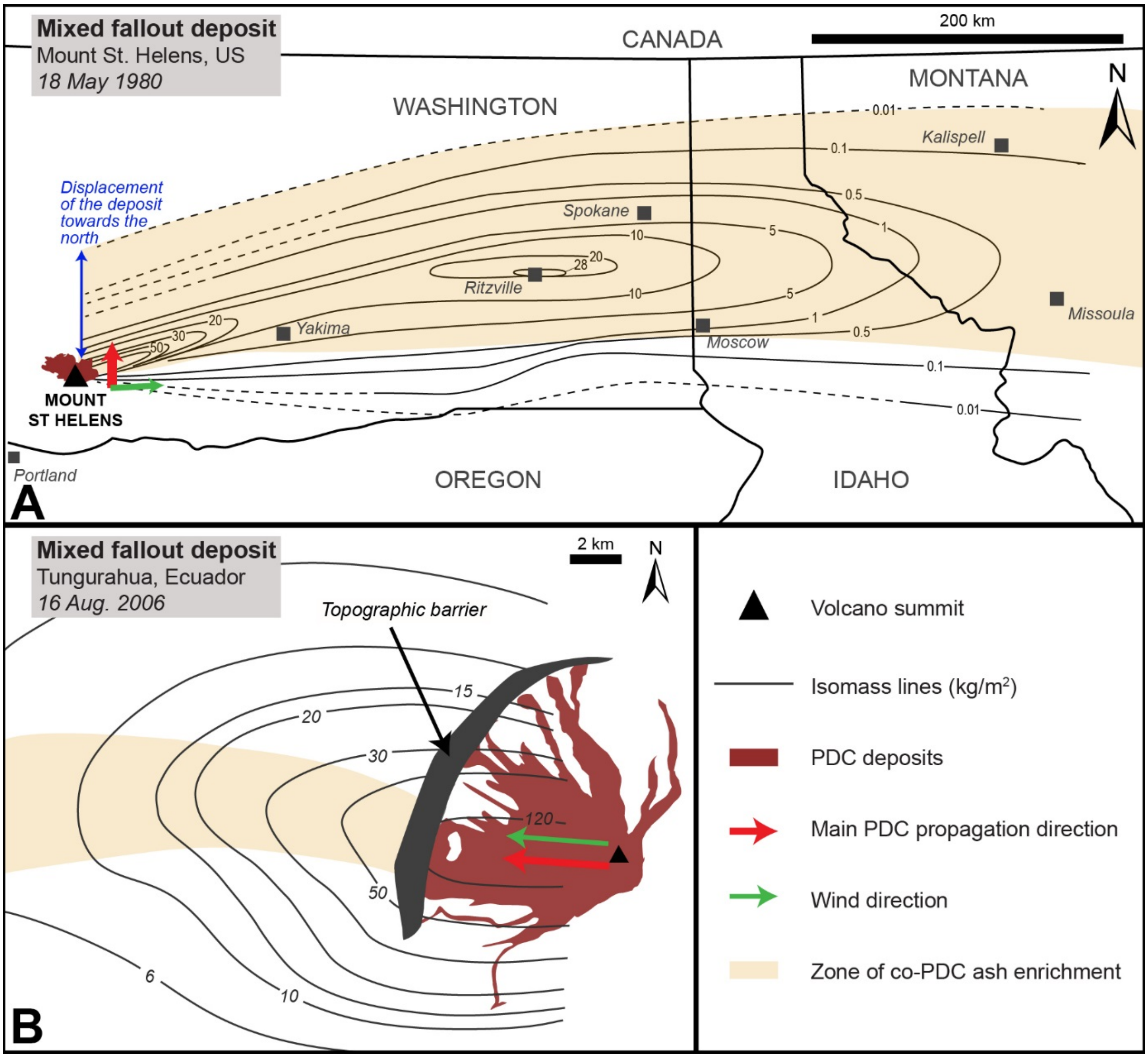

Figure 5. Dispersal of mixed fallout deposits from the May 18, 1980 Mount St. Helens (**A**) and August 16, 2006 Tungurahua (**B**) eruptions showing the effect of the co-PDC contributions on the geometry of the mixed deposits. Isomass lines from (**A**) Sarna-Wojcicki et al. (1981) and (**B**) Eychenne et al. (2013). **A.** Note the displacement of the overall deposit to the north of the vent (blue arrow) due to the northern momentum of the co-PDC plume generated by the blast. **B.** Note the steep high in topography (about 500 m to 1 km high) located perpendicular to the PDC propagation direction which enhanced the formation of co-PDC plumes.

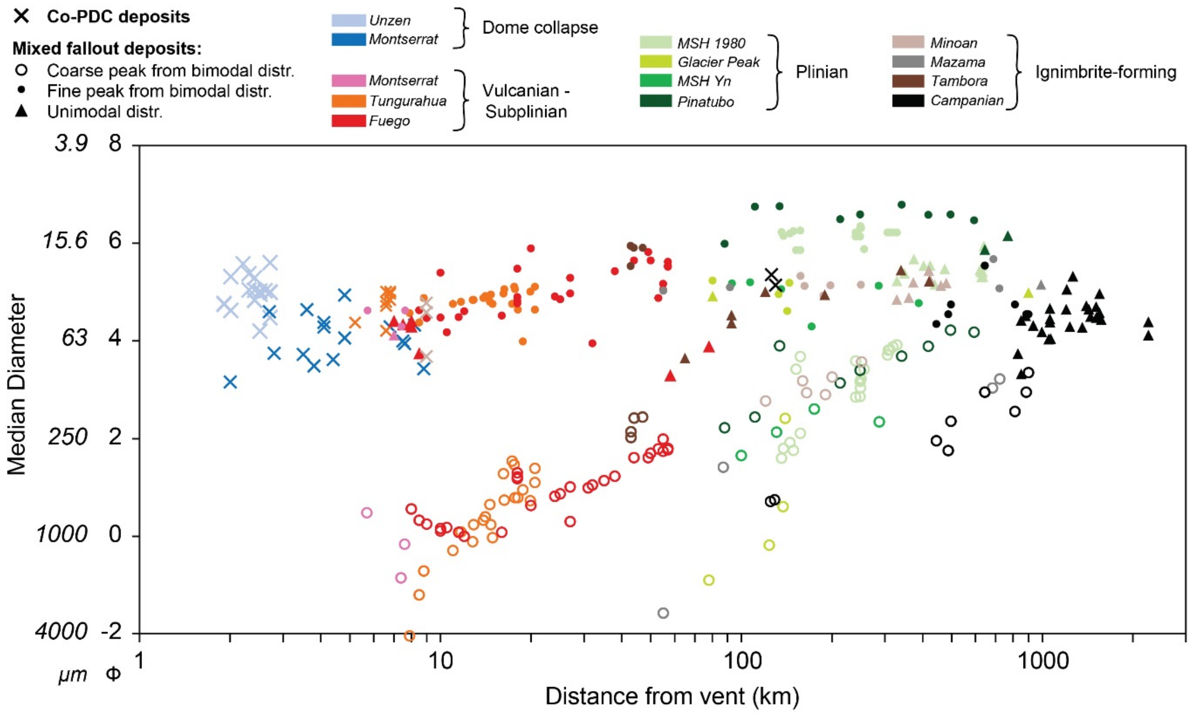

Figure 6. Grain size variations of co-PDC and mixed fallout deposits with distance from vent. The Median Diameter of the unimodal particle size distributions and coarse and fine grain size subpopulations of mixed fallout deposits are distinguished. See Table 1 for the list of eruptions and references.

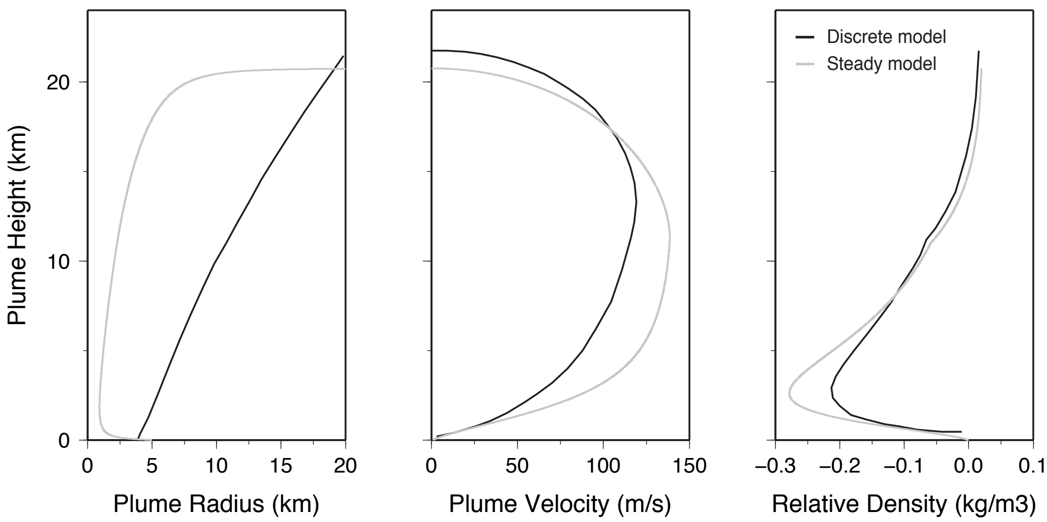

Figure 7. Comparison of model trends from the steady state plume model of Woods and Wohletz (1991), assuming an initial radius of 5 km, temperature of 832 K, an initial velocity of 1 m/s and initial plume density equal to that of the ambient, with the discrete buoyant thermal model of Woods and Kienle (1994), assuming an initial radius of 4 km and temperature of 700 K.

Table 1. Example of eruptions with

*	Magnitude data taken from LaMe
+	Converted volume bulk to DRE a
++	Converted from mass to volume

1 Watanabe et al, 1999
2 Miyabuchi, 1999
3 Bonadonna et al, 2002
4 Druitt et al, 2002
5 Eychenne et al, 2013
6 Bernard et al, 2014
7 Eychenne et al, 2012
8 Rose et al, 2008
9 Davies et al. 1978
10 Eychenne et al, submitted
11 Sarna-Wojcicki et al, 1981;
12 Hoblitt et al, 1981
13 Durant et al, 2009
14 Gardner et al. 1998
15 Beget 1983
16 Brazier et al. 1983
17 Carey & Sigurdsson, 1986
18 Macias et al, 1998
19 Rose & Durant, 2008
20 Carey et al. 1995
21 Wiesner et al, 2004
22 Scott et al, 1996
23 Sigurdsson et al 1990
24 Sparks & Huang 1980
25 Williams 1942
26 Williams and Goles 1968
27 Bacon 1983
28 Kandlbauer et al. 2014
29 Sigurdsson & Carey 1989
30 Pyle et al. 2006
31 Fisher et al. 1993
32 Engwell et al. 2014
33 Rose & Chesner 1987
34 Gatti and Oppenheimer 2012
35 Knight et al. 1986

associated coPDC deposits.

eve database:

ssuming a deposit density of 1000 kg/m^3

DRE assuming a solid density of 2500 (Mount St. Helens), 2600 (Tungurahua[l] and Mor ntserrat[v]) and 2200 kg/m^3 (Unzen[x])